Proton-driven spin diffusion in rotating solids via reversible and irreversible quantum dynamics

Mikhail Veshtort[a] and Robert G. Griffin[b]
Department of Chemistry and Francis Bitter Magnet Laboratory, Massachusetts Institute of Technology, Cambridge, Massachusetts 02139, USA

(Received 8 June 2011; accepted 15 August 2011; published online 7 October 2011)

Proton-driven spin diffusion (PDSD) experiments in rotating solids have received a great deal of attention as a potential source of distance constraints in large biomolecules. However, the quantitative relationship between the molecular structure and observed spin diffusion has remained obscure due to the lack of an accurate theoretical description of the spin dynamics in these experiments. We start with presenting a detailed relaxation theory of PDSD in rotating solids that provides such a description. The theory applies to both conventional and radio-frequency-assisted PDSD experiments and extends to the non-Markovian regime to include such phenomena as rotational resonance (R^2). The basic kinetic equation of the theory in the non-Markovian regime has the form of a memory function equation, with the role of the memory function played by the correlation function. The key assumption used in the derivation of this equation expresses the intuitive notion of the irreversible dissipation of coherences in macroscopic systems. Accurate expressions for the correlation functions and for the spin diffusion constants are given. The theory predicts that the spin diffusion constants governing the multi-site PDSD can be approximated by the constants observed in the two-site diffusion. Direct numerical simulations of PDSD dynamics via reversible Liouville-von Neumann equation are presented to support and compliment the theory. Remarkably, an exponential decay of the difference magnetization can be observed in such simulations in systems consisting of only 12 spins. This is a unique example of a real physical system whose typically macroscopic and apparently irreversible behavior can be traced via reversible microscopic dynamics. An accurate value for the spin diffusion constant can be usually obtained through direct simulations of PDSD in systems consisting of two ^{13}C nuclei and about ten ^{1}H nuclei from their nearest environment. Spin diffusion constants computed by this method are in excellent agreement with the spin diffusion constants obtained through equations given by the relaxation theory of PDSD. The constants resulting from these two approaches were also in excellent agreement with the results of 2D rotary resonance recoupling proton-driven spin diffusion (R^3-PDSD) experiments performed in three model compounds, where magnetization exchange occurred over distances up to 4.9 Å. With the methodology presented, highly accurate internuclear distances can be extracted from such data. Relayed transfer of magnetization between distant nuclei appears to be the main (and apparently resolvable) source of uncertainty in such measurements. The non-Markovian kinetic equation was applied to the analysis of the R^2 spin dynamics. The conventional semi-phenomenological treatment of relxation in R^2 has been shown to be equivalent to the assumption of the Lorentzian spectral density function in the relaxatoin theory of PDSD. As this assumption is a poor approximation in real physical systems, the conventional R^2 treatment is likely to carry a significant model error that has not been recognized previously. The relaxation theory of PDSD appears to provide an accurate, parameter-free alternative. Predictions of this theory agreed well with the full quantum mechanical simulations of the R^2 dynamics in the few simple model systems we considered. © *2011 American Institute of Physics*. [doi:10.1063/1.3635374]

I. INTRODUCTION

Spin diffusion in its various forms can be loosely defined as irreversible transport of spin order by the mutual flips of dipolar-coupled nuclei. First described by Bloembergen,[1] it has been studied by many authors over the years and is now ubiquitous in magnetic resonance experiments as a major mechanism for nuclear relaxation and as a common means to achieve polarization transfer. In the latter capacity, spin diffusion can be used to characterize the spatial proximity of the sites exchanging polarization and thus provides a way to correlate resonances for spectral assignments and to obtain direct structural information. Recently, these types of experiments have emerged as a particularly suitable approach for structural studies of membrane proteins, amyloid fibrils, and other biomolecular systems. In fact, spin diffusion experiments provided the key sets of distance constraints for majority of the protein structures determined with the solid-state

[a]Present address: Department of Biochemistry and Molecular Biophysics, Columbia University, 701 West 168th Street, New York, NY 10032, USA.
[b]Author to whom correspondence should be addressed. Electronic mail: rgg@mit.edu.

NMR methods.[2–8] In the light of these recent successes, and in the hopes of further refinement of these methods, spin diffusion presents a highly promising subject for detailed theoretical and quantitative exploration.

Two main classes of spin diffusion experiments are currently used to obtain structural constraints in the studies mentioned above. In one case, represented by the CHHC, NHHN, and NHHC experiments,[9–11] the magnetization exchange furnishing the structural information occurs between the proton nuclei, while it is initiated and detected via the low-gamma nuclei (^{13}C or ^{15}N). In the other case, known as the proton-driven spin diffusion (PDSD),[12–14] the polarization exchange occurs among the low-gamma nuclei, but its mechanism relies substantially on their coupling to the surrounding protons. The layout of the latter experiments and the way their results are incorporated into structure calculations closely resembles the NOESY protocol in liquids.[15,16] The primary difference is that the distance constraints obtained are among the low-gamma nuclei. (For the sake of brevity, we will refer to these nuclei as simply ^{13}C, although the statements will be also applicable to ^{15}N and possibly other nuclear species in general.)

The original PDSD experiments[12,13] were performed with no radio-frequency (RF) fields applied during the spin diffusion period. Costa *et al.*,[17] and subsequently others[18,19] have suggested applying a weak RF field at the proton frequency to increase the overall efficiency of the magnetization transfer. New names, RAD (RF assisted diffusion)[19] and DARR (dipolar-assisted rotational resonance),[18] were suggested for this experiment when the applied RF field satisfied the rotary resonance recoupling[20] (R^3) condition ($\omega_{RF} = \omega_R$ or $\omega_{RF} = 2\omega_R$). Although the name RAD is practical for distinguishing the two modes of conducting PDSD (with and without the ^{1}H RF field), we will use the term PDSD universally because applying RF at the proton frequency does not change the principal mechanism of the polarization transfer, as we demonstrate in the present work. With or without an applied RF field, PDSD is essentially a spin-spin relaxation process, as opposed to a coherent transfer due to a recoupled first[21–25] or second[26–28] order average Hamiltonian. Moreover, one can envision a whole class of RF-assisted PDSD experiments with diverse ^{1}H RF field sequences designed – possibly with the methodology described in the present work – to accommodate various experimental needs. Specific experiments in this class should probably have compound names such as R^3-PDSD and MIRROR-PDSD.[29]

Neither R^3-PDSD nor conventional (no-RF) PDSD experiments require high-power RF fields for either decoupling or recoupling, so very long mixing times may be used to achieve polarization transfer over relatively long distances. In addition, PDSD does not suffer from the dipolar truncation effect, where polarization transfer between weakly coupled nuclei is obstructed by the presence of strongly coupled nuclei.[30,31] The combination of these two features makes PDSD particularly promising for providing information on a wide range of interatomic distances. However, due to the lack of an accurate theoretical description of these experiments, the quantitative relationship between molecular structure and the observed spin diffusion has remained obscure.

A standard theoretical approach to the description of PDSD, since it is a relaxation process, would be with the methods that formally belong to the realm of the non-equilibrium statistical mechanics.[32] In this framework, the dynamics of a certain small set of "relevant" observables is described by an equation of motion that does not involve any other observables.[33] If this (kinetic) equation is exact, it must necessarily be non-Markovian. However, with the application of time coarse-graining it becomes Markovian and irreversible, and then it is usually referred to as a master equation. In the case of PDSD, the relevant degrees of freedom are assumed to be the longitudinal magnetizations $\langle I_{kz} \rangle$ of each participating ^{13}C (or ^{15}N) spin and the equation of motion is

$$\dot{\mathbf{M}}_z = \mathbf{W}\,\mathbf{M}_z, \tag{1}$$

where $\mathbf{M}_z$ is the column-vector of the magnetizations, and $\mathbf{W}$ is the matrix of spin diffusion rate constants, or the kinetic rate matrix.

Several authors have treated spin diffusion in terms of a master equation. Suter and Ernst[34] and Henrichs *et al.*[35] discussed PDSD in static solids. Kubo and McDowell[36] considered the case of rotating solids in magic angle spinning (MAS) experiments. In order to obtain quantitative estimates of the spin diffusion rate constants these authors had to resort to various, often very coarse approximations, particularly assuming a certain shape for the spectral density functions. Kubo and McDowell[36] also assumed that the spin diffusion constants do not depend on the orientation of the crystallite in the MAS rotor (while in reality they vary between zero and some maximum value).

While making this kind of approximations was helpful for obtaining qualitative insights, and, perhaps, was the best one could do at the time in terms of quantitative estimates, the situation has changed since then. The power of available computational resources has grown immensely and efficient numerical simulation software have been developed,[37] opening up new possibilities in approaching this problem. Two extreme strategies can be envisioned to this end. On one hand, one could try to simulate spin diffusion using the full (reversible) Liouville-von Neumann equation of motion, closely mimicking the actual experiment. One the other hand, one could rely on the master equation (1) with the spin diffusion rate constants obtained via numerically computed spectral density functions. If necessary, a suitable non-Markovian kinetic equation can be used instead of the master equation. These two approaches are complimentary in many ways, and we explore them both in this article, as well as a hybrid approach, where the spin diffusion constants are computed via direct simulations of the (reversible) PDSD dynamics. An implementation of the master equation strategy has been reported by Dumez and Emsley[38] while our manuscript was in preparation for publication. They have used numerically computed spectral densities but combined them with the approximate expressions for the spin diffusion constants given by Kubo and McDowell,[36] which lead to satisfactory but mixed results.

In spite of much progress in the area, numerical propagation of the density matrix on modern day computers cannot generally accommodate spin systems of more than

13 nuclei, unless one neglects the development of high order coherences.[39–42] Hence, it is not obvious *a priori* that exact numerical simulations should be generally effective for the description of spin diffusion in real experimental systems (in this study – biological solids). In peptides and proteins, the ^{1}H nuclei typically form a tightly coupled network extending throughout the whole protein or the whole crystal. The low-gamma nuclei are coupled to this network, which facilitates the exchange of their magnetization during PDSD. In this situation, it is not possible to identify a small isolated spin system where PDSD actually occurs. Thus, we are potentially facing at least two major problems with using exact simulations to model PDSD.

First, as commonly assumed in statistical mechanics, a typical macroscopic behavior (e.g., relaxation) can be observed only in a process that involves a bath with a very large number of degrees of freedom. In PDSD, these degrees of freedom are provided by the spin states of the protons. If one attempts a full quantum-mechanical description of this process, the bath must be included in the simulation as a part of the quantum-mechanical system. Thus, a model system for PDSD is expected to include a large number of protons, in addition to at least two, but typically many, low-gamma nuclei exchanging magnetization. Given the tight restrictions on the system size, it would seem unlikely that such simulations could successfully reproduce the relaxation dynamics of PDSD (i.e., Eq. (1)). To the best of our knowledge, this would be the first example of a real physical system, where a relaxation process can be simulated through reversible dynamics, i.e., in its full quantum mechanical detail.

Second, it is reasonable to assume that the protons nearest to the low-gamma nuclei exchanging magnetization have the greatest effect on the dynamics of the exchange. However, if the model system includes only the protons from the local environment, then a large number of strong dipolar interactions of these local protons with the remainder of the proton network are neglected, as well as a very large number of ^{13}C–^{1}H interactions that are of the same order of magnitude as most of the remaining ^{13}C–^{1}H interactions. This may potentially lead to inaccurate estimation of the spin diffusion constants or the exchange dynamics in general.

In what follows, we show that these potential issues are not insurmountable and that RF-assisted PDSD experiments in biological solids can be accurately simulated by both hybrid and the spectral densities methods. We present a careful theoretical and numerical exploration of various aspects of PDSD, which forms the basis for the methodology of the simulations and deepens our general understanding of this phenomenon, including its generalization to the non-Markovian regime. The theory applies without change to PDSD with a periodic ^{1}H RF field of any form. The experimental data presented are for 2D R^3-PDSD experiments in serine and two tripeptides, Gly-Gly-Val dihydrate (GGV) and Ala-Gly-Gly monohydrate (AGG). The simulations are limited to the cases of the conventional (no-RF) PDSD and the CW PDSD (constant phase and amplitude). Through numerical simulations, PDSD in rotating solids can be seen as a "macroscopic" process that can be studied in full microscopic detail via reversible dynamics. Although not pursued in the present work, recognition of this important fact may lead to the development of new models that enhance our understanding of various fundamental issues concerned with this duality, such as irreversibility,[43] ergodicity, quantum chaos,[44] decoherence,[45] entanglement,[45] and quantum computing.

II. THEORY

A. Spin diffusion between two nuclei

The rotating frame Hamiltonian of proton-driven spin diffusion between two ^{13}C nuclei in a MAS experiment includes the isotropic and anisotropic chemical shift, the dipolar coupling, and the radio-frequency field terms:

$$H(t) = H_{\mathrm{CS}}(t) + H_{\mathrm{D}}(t) + H_{\mathrm{RF}}, \tag{2}$$

$$H_{\mathrm{CS}}(t) = \sum_{i=1}^{2} \left(\omega_i^{\mathrm{iso}} + \omega_i^{\mathrm{CSA}}(t)\right) I_{1z} + \sum_i \left(\omega_i^{\mathrm{iso}} + \omega_i^{\mathrm{CSA}}(t)\right) S_{iz}, \tag{3}$$

$$\begin{aligned} H_{\mathrm{D}}(t) = {} & D_{2,0}^{\mathrm{CC}}(t)\frac{1}{\sqrt{6}}(3I_{1z}I_{2z} - \mathbf{I}_1 \cdot \mathbf{I}_2) \\ & + \sum_{i<j} D_{2,0}^{\mathrm{HH}[ij]}(t)\frac{1}{\sqrt{6}}(3S_{iz}S_{jz} - \mathbf{S}_i \cdot \mathbf{S}_j) \\ & + \sum_{i,j} D_{2,0}^{\mathrm{CH}[ij]}(t)\frac{2}{\sqrt{6}} I_{iz}S_{jz}, \end{aligned} \tag{4}$$

$$H_{\mathrm{RF}}(t) = \sum_i \omega_{\mathrm{RF}}(t)(S_{ix}\cos\phi(t) + S_{iy}\sin\phi(t)), \tag{5}$$

where $D_{2,0}^{\mathrm{CC}}(t)$, $D_{2,0}^{\mathrm{HH}[ij]}(t)$, and $D_{2,0}^{\mathrm{CH}[ij]}(t)$ are the $m = 0$ spherical components of the corresponding second-rank dipolar coupling tensors. Their time dependence due to MAS can be expressed as

$$D_{2,0}(t) = \sum_{k=-2}^{2} D_{2,0}^{(k)} e^{ik\omega_R t}, \tag{6}$$

with the vanishing $k = 0$ components and $D_{2,0}^{(-k)} = D_{2,0}^{(k)*}$. The values of the components depend on the orientation of the molecule in the MAS rotor and scale as r_{ij}^{-3}. The chemical shift anisotropy (CSA) terms in Eq. (3) are also proportional to $m = 0$ spherical components of orientation-dependent second-rank tensors and thus have the time dependence of the same form as the dipolar terms. The RF term (Eq. (5)) is assumed to be periodic, with the period of one rotor cycle (in general, it may simply be commensurate with the length of the rotor cycle). The isotropic ^{13}C–^{13}C J-coupling may also be present in the Hamiltonian. Its effects on spin diffusion are typically very small but may be non-negligible. The flip-flop (off-diagonal part) of J-coupling is identical to that of the dipolar coupling, while the diagonal part is irrelevant for the spin diffusion dynamics (see below). Therefore, if necessary, J-coupling can be accounted for through the $D_{2,0}^{(0)}$ component of $D_{2,0}(t)$.

The initial density matrix $\rho(0)$ and the observable are typically taken as the difference longitudinal magnetization of

the carbon spins, which we will denote as Q_z for brevity:

$$\rho(0) = I_{1z} - I_{2z} = Q_z. \tag{7}$$

For a qualitative understanding of the problem at hand, it is helpful to notice that it is equivalent to the problem of a single ^{13}C nucleus subjected to a weak RF field and coupled to a network of protons. Indeed, with the help of the fictitious spin notation,[46]

$$I_z^{(23)} = \frac{1}{2}(I_{1z} - I_{2z}), \tag{8}$$

$$I_z^{(14)} = \frac{1}{2}(I_{1z} + I_{2z}), \tag{9}$$

$$I_x^{(23)} = \frac{1}{2}(I_{1+}I_{2-} + I_{1-}I_{2+}), \tag{10}$$

etc., where the superscripts "23" and "14" refer to the two pairs of the four Zeeman basis states of the two-spin system, the Hamiltonian given by Eq. (2) can be written as

$$H(t) = \omega_\Delta^{\mathrm{CS}}(t)I_z^{(23)} + D(t)I_x^{(23)} + \sum_i D_i^{(23)}(t)I_z^{(23)}S_{iz} + H_{\mathrm{CS/H}}(t) + H_{\mathrm{HH}}(t) + H_{\mathrm{RF}}(t), \tag{11}$$

where

$$\omega_\Delta^{\mathrm{CS}}(t) = \left(\omega_1^{\mathrm{iso}} - \omega_2^{\mathrm{iso}}\right) + \left(\omega_1^{\mathrm{CSA}}(t) - \omega_2^{\mathrm{CSA}}(t)\right) = \omega_\Delta^{\mathrm{iso}} + \omega_\Delta^{\mathrm{CSA}}(t), \tag{12}$$

$$D(t) = \sqrt{6}D_{2,0}^{\mathrm{CC}}(t), \tag{13}$$

$$D_i^{(23)}(t) = \frac{1}{\sqrt{6}}\left(D_{2,0}^{\mathrm{CH}[i1]}(t) - D_{2,0}^{\mathrm{CH}[i2]}(t)\right), \tag{14}$$

$$H_{\mathrm{HH}}(t) = \sum_{i<j} D_{2,0}^{\mathrm{HH}[ij]}(t)\frac{1}{\sqrt{6}}(3S_{iz}S_{jz} - \mathbf{S}_i \cdot \mathbf{S}_j). \tag{15}$$

The "14" part of the $H_{\mathrm{CS}}(t)$ term,

$$H_{\mathrm{CS}}^{(14)}(t) = \omega_\Sigma^{\mathrm{CS}}(t)I_z^{(14)}, \tag{16}$$

the $I_{1z}I_{2z}$ part of the $H_{\mathrm{CC}}(t)$ term, and the "14" parts of $H_{\mathrm{CH}}(t)$ are not included in Eq. (11) since they commute with the rest of the Hamiltonian, as well as with the observable,

$$Q_z = 2I_z^{(23)}, \tag{17}$$

and, therefore, do not affect the signal. The term involving $I_x^{(23)}$ can be interpreted as a sum of two RF fields, applied with the offsets ω_R and $2\omega_R$ (see Eq. (6)). In the absence of the protons, Eq. (11) becomes the off-rotational resonance Hamiltonian,[46] which would become resonant when $\omega_\Delta^{\mathrm{iso}}$ equals ω_R or $2\omega_R$. In the presence of a single proton, Eq. (11) becomes a DARR model Hamiltonian.[18,47] In the presence of multiple protons but in the absence of $H_{\mathrm{HH}}(t)$, it becomes a multi-proton DARR Hamiltonian. However, the H–H couplings present in the full PDSD Hamiltonian completely change the dynamics, making it of the relaxation type rather than coherent and rendering all above-mentioned simple models inapplicable in this situation. Qualitatively, one can see from Eq. (11) that the dynamics will be that of a single spin in the presence of weak RF and strong transverse relaxation.

In order to obtain a correct kinetic equation for PDSD, we will use the interaction frame defined by the following sum of terms:

$$H_0(t) = H_{\mathrm{CS}}(t) + H_{\mathrm{CH}}(t) + H_{\mathrm{HH}}(t) + H_{\mathrm{RF}}(t), \tag{18}$$

which includes all terms of the rotating frame Hamiltonian except for the C–C dipolar coupling:

$$H(t) = H_0(t) + H_1(t), \tag{19}$$

$$H_1(t) = D(t)I_x^{(23)}. \tag{20}$$

In this frame, the Hamiltonian becomes

$$H_I(t) = U_0^\dagger(t)H_1(t)U_0(t), \tag{21}$$

$$U_0(t) = T\exp\left\{-i\int_0^t H_0(t_1)\,dt_1\right\}, \tag{22}$$

where T is the Dyson time-ordering operator. The time evolution in the rotating frame can then be computed as

$$U(t) = U_0(t)U_I(t), \tag{23}$$

$$U_I(t) = T\exp\left\{-i\int_0^t H_I(t_1)\,dt_1\right\}. \tag{24}$$

Since $H_0(t)$ and, therefore, $U_0(t)$ commute with Q_z, the expression for the signal is

$$s(t) = \frac{1}{Tr\left(Q_z^2\right)}Tr\left(\rho(t)Q_z\right) = \frac{1}{Tr\left(Q_z^2\right)}Tr\left(U_I(t)Q_zU_I^\dagger(t)Q_z\right). \tag{25}$$

In other words, the interaction frame density matrix can be used to compute the signal instead of the rotating frame density matrix.

With this definition of the signal, the density matrix at any time can be represented as a sum of two orthogonal terms:

$$\rho(t) = s(t)\,Q_z + R(t), \tag{26}$$

$$\langle Q_z|R(t)\rangle = 0, \tag{27}$$

where we have used the standard Liouville space definition of the scalar product,

$$\langle A|B\rangle = Tr(A^\dagger B). \tag{28}$$

As the evolution is coherent and unitary, the norm of the density matrix (equal to the sum of absolute squares of all its matrix elements) is constant. In view of the orthogonality of the two terms,

$$\|\rho(t)\|^2 = \|s(t)Q_z\|^2 + \|R(t)\|^2 = \|Q_z\|^2. \tag{29}$$

Equation (29) shows that, as the signal decays, polarization flows from the Q_z term to the $R(t)$ term. In a system with many protons, it spreads, through the mediation of dipolar couplings, over a very large number of coherences in $R(t)$. It appears that this dissipation of coherences is the fundamental source of irreversibility of the spin diffusion. We will formulate this statement in more precise terms below.

If the Liouville-von Neumann equation,

$$\frac{d}{dt}\rho(t) = -i[H(t),\ \rho(t)], \tag{30}$$

is integrated on both sides from 0 to t, and the resulting expression for $\rho(t)$ is substituted back into Eq (30), one obtains the (exact) second-order iterated expansion for its derivative:

$$\frac{d}{dt}\rho(t) = -i[H(t), \rho(0)] - \left[H(t), \int_0^t [H(t_1), \rho(t_1)]dt_1\right]. \tag{31}$$

We will use this expression, in the interaction frame defined above, to compute the time evolution of the signal:

$$\frac{d}{dt}s(t) = \frac{1}{\|Q_z\|^2} Tr\left(Q_z \frac{d}{dt}\rho_I(t)\right)$$
$$= -\frac{1}{\|Q_z\|^2}\int_0^t Tr(Q_z[H_I(t), [H_I(t_1), s(t_1)Q_z + R_I(t_1)]])dt_1. \tag{32}$$

Note that the first-order term vanished due to the identity

$$Tr(A[B, A]) = 0. \tag{33}$$

The $R_I(t)$ term may be large, as measured by its norm (cf. Eq. (29)), but if it is spread over a large number of coherences, its contribution to the integral in Eq. (32) is likely to be negligible. Obviously, the distribution of $R_I(t)$ over the various coherences will not be uniform and will vary with time. Most notably, the ^{13}C zero-quantum coherences, appearing in the first-order term in the perturbation expansion of $\rho_I(t)$, will be present in significant quantities in $R_I(t)$ throughout the whole time of exchange. However, one can show that in the interaction frame chosen, these coherences, together with all odd order terms in the perturbation expansion of $\rho_I(t)$ will have identically vanishing contributions to the integral in Eq. (32). As no other coherences can be suspected in significantly contributing to this integral, it is reasonable to assume that $R_I(t)$ can be neglected altogether. This assumption is justified by the agreement of the results of the theory with the experimental data and with the direct simulations, as will be shown below. However, the exact conditions of its validity still remain to be established. In particular, this issue can be explored in detail with the help of numerical simulations. The importance of the dissipation of coherences is further illustrated in Sec. VI E.

Thus, neglecting $R_I(t)$, we obtain

$$\frac{d}{dt}s(t) = -\int_0^t \Phi(t;\tau)\, s(t-\tau)\, d\tau, \tag{34}$$

where

$$\Phi(t;\tau) = \frac{1}{\|Q_z\|^2} Tr\big(Q_z\big[H_I(t),\ [H_I(t-\tau),\ Q_z]\big]\big). \tag{35}$$

We will call $\Phi(t;\tau)$ a correlation function as it has the form $\langle C(t)|C(t-\tau)\rangle$, which can be seen by rearranging the commutators in Eq. (35). Under the condition that $\Phi(t;\tau)$ decays faster than the signal has time to change noticeably, $s(t)$ can be taken outside of the integral in Eq. (34). In addition, the upper integration limit can be extended to infinity if $t \gg \tau_c$, where τ_c is the characteristic decay time (correlation time). Assuming that these two conditions are fulfilled, we have

$$\frac{d}{dt}s(t) = -s(t)\int_0^\infty \Phi(t;\tau)d\tau. \tag{36}$$

As we will see later, $\Phi(t;\tau)$ is periodic in t, with the period of one rotor cycle, τ_R. Hence, if we observe the average of $s(t)$ over a rotor cycle, it will decay exponentially, with the constant given by the average of the $\Phi(t;\tau)$ integral:

$$k_D = \frac{1}{\tau_R}\int_0^\infty \int_0^{\tau_R} \Phi(t;\tau)dtd\tau. \tag{37}$$

Note that in the derivation above we did not make any assumptions about the "bath" being in a state of thermal equilibrium and never becoming entangled with the observed system, or about the accuracy of any second-order perturbation expansions, which are typical for the traditional spin relaxation theory.[48,49] The non-Markovian kinetic equation (34) was obtained based on a single assumption discussed above, while the Markovian equation (36) was obtained with the help of two additional assumptions that are ubiquitous in the relaxation theory. An alternative formulation of the assumptions leading to the Markovian equation (via the Fourier or Laplace transform of Eq. (34)) will be given later, in Sec. VI D. Note that Eq. (34) is similar to the memory function equation derived using the projection operator technique,[33] but it approximates the difficult to compute memory function with the correlation function $\Phi(t;\tau)$ that can be readily computed numerically.

By substituting the specific expressions for the Hamiltonian (Eqs. (20) and (21)) and Q_z (Eq. (17)) into Eq. (35), recalling that $U_0(t)$ commutes with $I_z^{(23)}$, rearranging the commutators under the trace, and performing some simple algebraic transformations (see Eq. (B1), Appendix B), we obtain the following expression for the correlation function:

$$\Phi(t;\tau) = \frac{1}{\left\|I_z^{(23)}\right\|^2} D(t)D(t-\tau) \times Tr\big(I_y^{(23)}U_0(t, t-\tau)I_y^{(23)}U_0^\dagger(t, t-\tau)\big). \tag{38}$$

$U_0(t, t-\tau)$ in Eq. (38) is the propagator from time $t-\tau$ to time t. We further transform this equation by shifting t by τ on both sides and using the identity

$$Tr(I_y U I_y U^\dagger) = \frac{1}{4}Tr(I_- U I_+ U^\dagger) + \text{c.c.}, \tag{39}$$

where c.c. is the complex conjugate of the preceding term. The resulting equation,

$$\Phi(t+\tau;\tau) = \frac{1}{4\left\|I_z^{(23)}\right\|^2} D(t+\tau)D(t) \times Tr\big(I_-^{(23)}U_0(t+\tau, t)I_+^{(23)}U_0^\dagger(t+\tau, t)\big) + \text{c.c.}, \tag{40}$$

now contains propagators in the form more appropriate for expressing $\Phi(t;\tau)$ through the zero-quantum coherence decay (see Eq. (44) below).

The evolution due to the ^{13}C isotropic chemical shift and CSA differences in Eq. (40) can be computed analytically, as they can be factored out of U_0:

$$U_0(t+\tau, t) = \exp\left\{-i\tau\omega_\Delta^{\text{iso}} I_z^{(23)}\right\} \times \exp\left\{-i(\phi(t+\tau) - \phi(t))I_z^{(23)}\right\}U_{\text{H}}(t+\tau, t), \tag{41a}$$

$$U_0(t+\tau, t) = \exp\left\{-i\tau\omega_\Delta^{\text{iso}} I_z^{(23)}\right\} U'_{\text{H}}(t+\tau, t), \tag{41b}$$

where

$$\phi(t) = \int_0^t \omega_\Delta^{\mathrm{CSA}}(t')\,dt', \tag{42}$$

is a periodic accumulated phase function, conveniently parameterized as

$$\exp\{i\phi(t)\} = \sum_{k=-\infty}^{+\infty} C^{(k)} e^{ik\omega_R t}. \tag{43}$$

The Fourier coefficients in Eq. (43) are most readily computed numerically, as a spectrum of the single quantum coherence evolution due to CSA. An explicit series expansion into Bessel functions is also available for these coefficients.[50,51]

The evolution due to the remaining terms of $H_0(t)$ (RF, CS/H, CH, and HH) can be described via the function

$$G(t;\tau) = \frac{1}{\|I_+^{(23)}\|^2} Tr\left(I_-^{(23)} U_{\mathrm{H}}(t+\tau,t) I_+^{(23)} U_{\mathrm{H}}^{\dagger}(t+\tau,t)\right), \tag{44}$$

which is the decay of the ^{13}C zero-quantum coherence, normalized to one for $\tau = 0$. Since $H_0(t)$ is periodic, $G(t;\tau)$ is also periodic in t. We will use the following notation for the Fourier expansions of $G(t;\tau)$:

$$G(t;\tau) = \sum_{k=-\infty}^{+\infty} G_k(\tau) e^{ik\omega_R t}, \tag{45}$$

$$J_k(\omega) = \int_0^{\infty} G_k(\tau) e^{-i\omega\tau} d\tau. \tag{46}$$

Substitution of Eqs. (6), (13), (41a), and (43)–(45) into Eq. (40), followed by a $t \to t - \tau$ time shift (see Appendix A for details), yields the following expression for $\Phi(t;\tau)$:

$$\Phi(t;\tau) = \frac{1}{2} \sum_{k,m,n} \omega_D^{(n)} \omega_D^{(n+k-m)*} e^{im\omega_R t} \times e^{-i(\omega_\Delta^{\mathrm{iso}} - n\omega_R + m\omega_R)\tau} G_k(\tau) + \mathrm{c.c.}, \tag{47}$$

where

$$\omega_D^{(n)} = \frac{1}{\sqrt{6}} \sum_{k=-2}^{2} D_{2,0}^{(k)} C^{(k-n)*}. \tag{48}$$

Integration over t and τ gives an expression for the decay constant:

$$k_D = \frac{1}{2} \sum_{n,k} \omega_D^{(n)} \omega_D^{(n+k)*} J_k\left(\omega_\Delta^{\mathrm{iso}} - n\omega_R\right) + \mathrm{c.c.} \tag{49}$$

The quantities $\omega_D^{(n)}$ can be recognized as the Fourier components of the effective dipolar Hamiltonian in rotational resonance.[46,52,53] If Eq. (41b) is used instead of Eq. (41a), one obtains

$$k_D = \frac{1}{12} \sum_{n,m=-2}^{2} D_{2,0}^{(n)} D_{2,0}^{(m)*} J'_{-n+m}\left(\omega_\Delta^{\mathrm{iso}} - n\omega_R\right) + \mathrm{c.c.} \tag{50}$$

In this form of the equation for k_D, the CSA effects are described through $J'_k(\omega)$. If these effects are absent or negligible, then $J'_k(\omega)$ coincides with $J_k(\omega)$ and Eq. (49) becomes Eq. (50). As mentioned above, if the isotropic ^{13}C–^{13}C J-coupling is absent or neglected, the Fourier coefficient $D_{2,0}^{(0)}$ is zero at the exact magic angle. Otherwise, the J-coupling can be accounted for by using $2\pi\sqrt{6}J_{\mathrm{iso}}$ for the $D_{2,0}^{(0)}$ value. Note that the $J_0(\omega)$'s contribution to k_D is

$$k_D^{(0)} = \sum_n \left|\omega_D^{(n)}\right|^2 \mathrm{Re} J_0\left(\omega_\Delta^{\mathrm{iso}} - n\omega_R\right). \tag{51}$$

If the Hamiltonian of the propagator U_H, did not contain the ^{1}H CS terms, it would be invariant with respect to the transformation with the unitary operator

$$K = 2I_{1x} 2I_{2x} \prod_k 2S_{kx}, \tag{52}$$

which interchanges the $|\alpha\rangle$ and $|\beta\rangle$ states for each spin. We can use this symmetry to show then that $G(t;\tau)$ is purely real: By transforming all operators under the trace in Eq. (44) with K and then transposing the product, one obtains

$$G(t;\tau) = \frac{1}{\|I_+^{(23)}\|^2} Tr\left(U_{\mathrm{H}}^{*}(t+\tau,t) I_+^{(23)} U_{\mathrm{H}}^{T}(t+\tau,t) I_-^{(23)}\right), \tag{53}$$

which is identical with $G^*(t;\tau)$ as can be seen by comparing with Eq. (44). It follows then that

$$G_k(\tau) = G_{-k}^*(\tau), \tag{54}$$

$$J_k(\omega) = J_{-k}^*(-\omega). \tag{55}$$

Note that these symmetries are dependent on the assumption that $H_0(t)$ does not contain the ^{1}H chemical shifts. In real physical systems, these terms are present but their effects on the zero-quantum lineshapes are small, entailing that Eqs. (54) and (55) should be seen as approximations. $J'_k(\omega)$ does not have these symmetries as it contains the effects of the ^{13}C CSAs.

B. Multi-site spin diffusion

The equations for the spin diffusion among multiple sites can be obtained using a similar approach. The observables now are the I_{kz} operators, the signal is given by the set of functions

$$s_k(t) = \frac{1}{\|I_{kz}\|^2} Tr(\rho(t) I_{kz}), \tag{56}$$

and the density matrix is represented (via orthogonal projections onto I_{kz} operators) as

$$\rho(t) = \sum_k s_k(t) I_{kz} + R(t). \tag{57}$$

The Hamiltonian now includes the chemical shift interactions for all ^{13}C spins and the dipolar interactions of all possible spin pairs in the system. In particular, Eq. (20) becomes

$$H_1(t) = \sum_{k<l} D_{kl}(t) I_x^{kl(23)}. \tag{58}$$

The Hamiltonian commutes with the sum I_{kz}, implying that this sum is conserved in spin diffusion.

Substituting Eq. (57) into Eq. (31) and neglecting $R_I(t)$ under the integral, we obtain

$$\frac{d}{dt}s_k(t) = -\sum_l \int_0^\infty \Phi_{kl}(t;\tau)s_l(t-\tau)d\tau. \quad (59)$$

The correlation functions expressions,

$$\Phi_{kl}(t;\tau) = -\frac{1}{\|I_{kz}\|^2}D_{kl}(t)D_{kl}(t-\tau) \times Tr\left(I_y^{kl(23)}U_0(t,t-\tau)I_y^{kl(23)}U_0^\dagger(t,t-\tau)\right), \quad (60)$$

(for $k \neq l$) and

$$\Phi_{kk}(t;\tau) = \frac{1}{\|I_{kz}\|^2}\sum_l D_{kl}(t)D_{kl}(t-\tau) \times Tr\left(I_y^{kl(23)}U_0(t,t-\tau)I_y^{kl(23)}U_0^\dagger(t,t-\tau)\right), \quad (61)$$

are derived in Appendix B. The Markovian master equation (Eq. (1)) follows from Eq. (59) after making two assumptions analogous to the two-spin case.

Applying Eq. (60) to a system with only two sites and comparing with Eq (38), one can see that

$$\Phi(t;\tau) = -2\Phi_{12}(t;\tau) = 2\Phi_{11}(t;\tau) = 2\Phi_{22}(t;\tau), \quad (62)$$

where the factor of two comes from

$$\|I_{kz}\|^2 = 2\|I_z^{kl(23)}\|^2. \quad (63)$$

To avoid confusion, we will use the following notation:

$$\frac{d}{dt}s_k(t) = \sum_l w_{kl}s_l(t), \quad (64)$$

$$w_{kl} = -\frac{1}{\tau_R}\int_0^\infty\int_0^{\tau_R}\Phi_{kl}(t;\tau)dtd\tau, \quad (65)$$

reserving the term "spin diffusion rate constant," or simply the "spin diffusion constant" for the quantities w_{kl}. The quantities k_D, defined by Eq. (37) and related to w_{kl} as

$$k_D^{(kl)} = 2w_{kl}, \quad (66)$$

(according to Eq. (62)) will be called the "decay constants," implying the exponential decay of the difference magnetization in a system with two ^{13}C nuclei. Equations. (62) and (66) are consequences of the fact that the eigenvalues of the spin diffusion rate matrix for two-site exchange are zero and $-2w_{12}$. The former represents the rate of change of the sum magnetization, and the latter – of the difference magnetization.

Thus, in a system with only two spin diffusion sites, we obtain exactly same dynamics as before. However, in a system with multiple sites, propagators $U_0(t,t-\tau)$ in Eqs. (38) and (60) will not be the same due to additional C–H dipolar coupling terms present in $H_0(t)$. Nevertheless, this difference does not appear to be very significant. Indeed, the trace in Eq. (60) can be represented as a sum over all possible states of the ^{13}C spins other than k and l. Each term in this sum will be a trace identical to the one appearing in Eq. (38), except that its propagators contain the effects of these additional C–H coupling terms, which have the form of ^{1}H CSA interactions. As discussed below (Sec. VI B), we found that the effects of ^{1}H CSA interactions on R^3-PDSD dynamics were very small in all our test cases. It also seems reasonable to assume that this will be true in general, although the accuracy of this approximation may depend on the specific PDSD experiment. The CSA-like terms due to the CH couplings are different only in that their size for directly bonded CH pairs is about 21 kHz, which is much larger than the typical authentic ^{1}H CSA's. However, such terms can be encountered only for protons that are not directly bonded to the spins k and l, so the effects of these relatively large terms on spin diffusion are still likely to be small. For the protons directly bonded to spins k and l, these effective CSA terms will be typically under 3 kHz. Thus, it appears that $\Phi_{kl}(t;\tau)$ and w_{kl} are not significantly affected by the presence of other ^{13}C spins in the system and can be computed using the expressions derived for the two-site spin diffusion.

It follows from Eqs. (60), (61), and (65) that the diagonal elements of the spin diffusion rate matrix $\mathbf{W}$ can be computed as follows:

$$w_{kk} = -\sum_l w_{kl}, \quad (67)$$

which is consistent with the conservation of the total z-magnetization during spin diffusion. Note that if we excluded one or more spins from the set of relevant observables in the derivation above, Eq. (61) would still contain the terms for the missed spins, leading to an apparent non-conservation of the total magnetization.

C. Accounting for spin-lattice relaxation

Relaxation of the ^{13}C longitudinal polarizations due to coupling to the lattice vibrations is often significant during PDSD experiments, in which case it must be taken into account. Assuming that relaxation and spin diffusion are independent, and that the ^{13}C nuclei do not cross-relax, the longitudinal magnetizations should obey the following equation in the presence of relaxation:

$$\dot{\mathbf{M}}_z = \mathbf{W}\,\mathbf{M}_z - \mathbf{R}\left(\mathbf{M}_z - \mathbf{M}_z^0\right), \quad (68)$$

where $\mathbf{R}$ is the diagonal relaxation matrix, and $\mathbf{M}_z^0$ is the vector of quasi-equilibrium magnetizations for the given experimental conditions, i.e., the RF field applied at the proton frequency, the spinning frequency, etc. Note that due to the nuclear Overhauser effect, $\mathbf{M}_z^0$ is different from the vector of equilibrium magnetizations for the unperturbed system. The solution to the inhomogeneous linear Eq. (68) for the initial condition $\mathbf{M}_z(0)$ can be represented as

$$\mathbf{M}_z(t) = \Delta\mathbf{M}_z(t) + \mathbf{M}_z^{\mathrm{st}}, \quad (69)$$

where $\mathbf{M}_z^{\mathrm{st}}$ is the stationary solution of Eq. (68), and $\Delta\mathbf{M}_z(t)$ is the solution to the homogeneous part of Eq. (68) that satisfies Eq (69) at $t = 0$:

$$\Delta\mathbf{M}_z(t) = e^{(\mathbf{W}-\mathbf{R})t}(\mathbf{M}_z(0) - \mathbf{M}_z^{\mathrm{st}}). \quad (70)$$

Hence, $\mathbf{M}_z(t)$ can be expressed as follows:

$$\mathbf{M}_z(t) = e^{(\mathbf{W}-\mathbf{R})t}\mathbf{M}_z(0) + (\mathbf{1} - e^{(\mathbf{W}-\mathbf{R})t})\mathbf{M}_z^{\mathrm{st}}. \quad (71)$$

In a 2D PDSD experiment, the first term of Eq. (71) is modulated by the evolution in the indirect dimension, while the second term is constant (for fixed mixing time), giving rise to peaks at zero frequency (axial peaks). By using a two-step phase cycle that alternates the sign of $\mathbf{M}_z(0)$, the second term is suppressed and only the first term is detected in the experiment. Furthermore, a 2D PDSD experiment can be described in terms of the set of initial magnetizations given by the columns of the unit matrix of the size equal to the number of sites exchanging magnetization. The idealized signal in such an experiment is then represented by the following matrix:

$$\mathbf{s}(t) = e^{(\mathbf{W}-\mathbf{R})t}, \tag{72}$$

which must also be averaged over all possible orientations present in the sample.

III. DIRECT SIMULATIONS OF PDSD

We start with exploring the question of whether it is possible to observe the exponential decay of the difference magnetization (expected for a macroscopic system) in spin systems amenable to numerical simulations of their full (reversible) quantum dynamics. Figure 1 shows simulations of the magnetization exchange between C_α and C_β of serine coupled to 5 to 10 nearest ^{1}H nuclei during R^3-PDSD in a single crystal. The decay curves converge to an exponential decay as the number of protons in the system is increased. The exponential character of the curves can be evaluated on the semilogarithmic plot in Fig. 1(b). The initial decay rate is essentially the same for all curves, which means that the decay constant can be extracted from such simulations in relatively small spin systems in this case. The exponential decay stops when a certain degree of magnetization transfer is reached. It is then followed by chaotic oscillations of magnetization around some constant value. The amplitude and the mean of these oscillations decrease with the number of protons in the system (Fig. 1(c)). The 10-proton curve starts to deviate from the exponential character after decaying to about 3% of the initial magnetization in this system.

Figure 2 shows the simulations of exactly the same spin systems in a PDSD experiment with no RF field applied at the ^{1}H frequency. The same general features as were seen in Fig. 1, can be observed in these plots as well. The main differences are that the decay is slightly slower, and more protons are necessary for a system in the no-RF experiment to exhibit a curve of comparable exponential character.

Important additional features of the exchange can be seen in Fig. 3, where only the first seven rotor cycles are shown (with the curves finely sampled) and the exchange is between the Val carboxyl and the Gly 1 carbonyl of GGV for two crystallite orientations that differ only by the value of the Euler angle γ, which specifies the rotation of the crystallite about the rotor axis. The correlation time for the zero-quantum coherence decay in a pair of carbons with no directly bonded protons is obviously much longer than in other kinds of pairs. A CO–CO pair was chosen for this example so that the initial, non-stationary phase of the decay would be clearly seen; in other systems, this phase is typically shorter and less pronounced. The oscillations of the curves are due to large CSAs. After the chaotic initial phase is over, the small periodic oscillations continue (in agreement with Eq. (36)), while the cycle average of the magnetization decays exponentially. Because the non-stationary phase outcome depends on the angle γ, the cycle-averaged curves are shifted with respect to each other for different γ values, even though they have exactly the same decay rates. The decay constant can be readily estimated by computing the degree of decay at some time t, which is sufficiently short so that the decay is still exponential but is

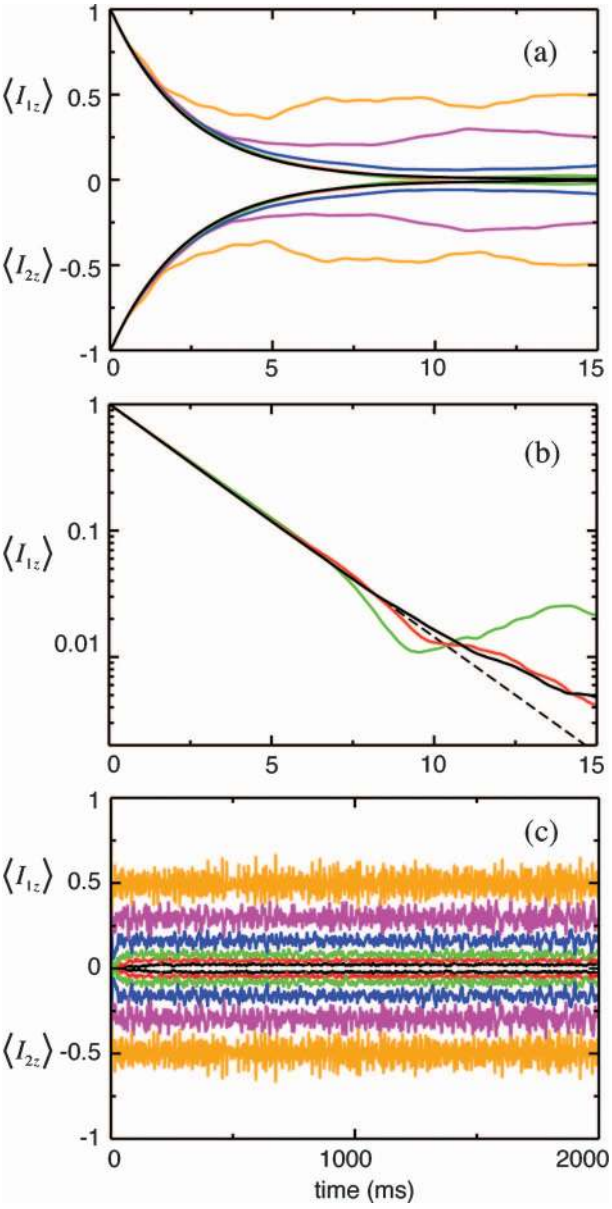

FIG. 1. Magnetization exchange between C_α and C_β in serine during R^3-PDSD computed with 5 (orange), 6 (magenta), 7 (blue), 8 (green), 9 (red), and 10 (black) nearest protons in the spin system (for a single crystallite). Magnetizations are normalized to give a unit signal at $t = 0$. The initial decay (a), the initial decay on the logarithmic scale (b), and the long-term behavior (c) are shown; the dashed black curve in (b) is a straight line shown for visual enhancement; only 8, 9, and 10-proton systems are shown in (b). The angle between the C–C axis and the rotor axis is 45°. The spinning frequency and the ^{1}H RF field are 10 kHz. The -NH_3 group exchange is frozen. The choice of the nearest protons and other details of the simulations are explained in the Sec. V.

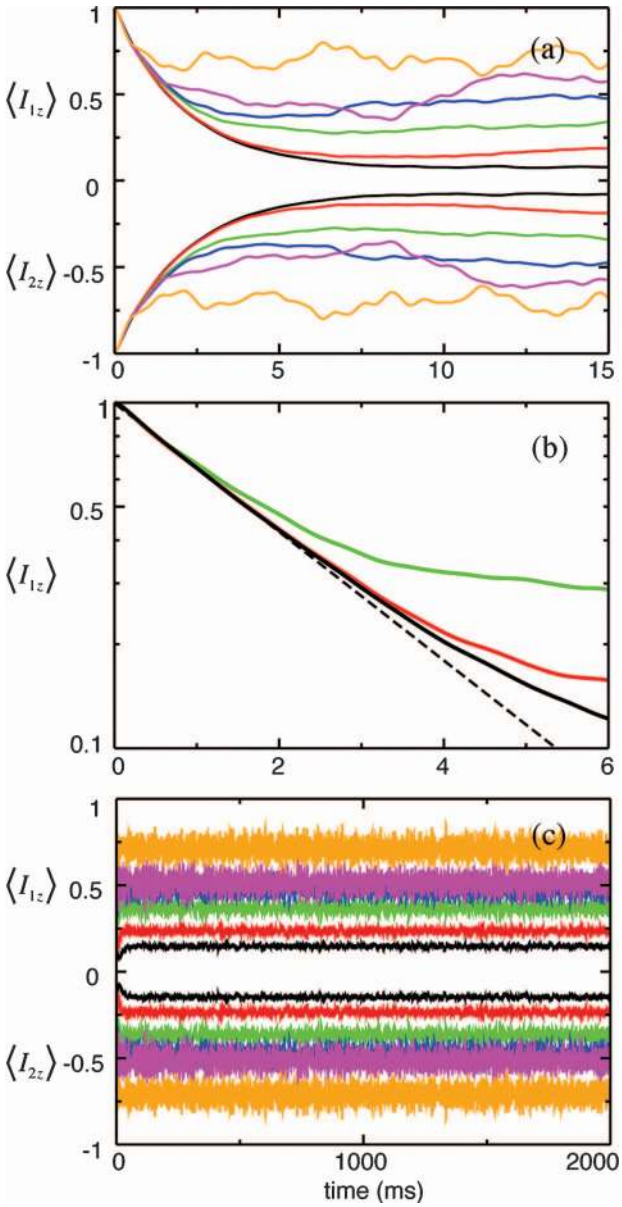

FIG. 2. Magnetization exchange in conventional PDSD. Conditions are the same as for Fig. 1, except that no ^{1}H-resonant RF field is applied during the spin diffusion.

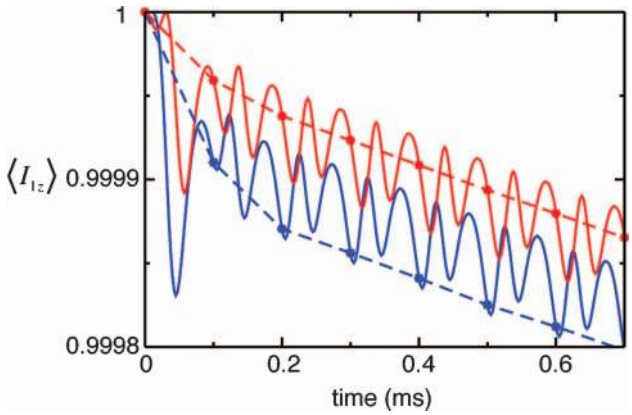

FIG. 3. A detailed view of the magnetization exchange at the beginning of R^3-PDSD. The solid lines show $\langle I_{1z}\rangle$ behavior for two different values of the Euler angle γ; the α and β angles are the same. The asterisks mark the points sampled at the end of every revolution of the rotor; the dashed lines connect these points for visual enhancement. Magnetizations are normalized to give a unit signal at $t = 0$. The spin system is a GGV fragment consisting of Gly 1 carbonyl, Val 3 carboxyl, and 8 nearest protons; the dipolar coupling between the ^{13}C nuclei was scaled by a factor of two. The angle between the C–C axis and the rotor axis is 45°. The spinning frequency and the ^{1}H RF field are 10 kHz.

sufficiently long so that the transfer during the non-stationary phase can be neglected compared to the overall decay. The accuracy of such an estimate turns out to be sufficient for the simulations of orientational averages. For more precise estimates of the constants, two points on the decay curves must be computed.

The stationary values around which the magnetizations oscillate in the long time limit depend not only on the number of protons in the system as seen in Figs. 1 and 2 but on other factors as well. In particular, they increase if the C–C and C–H dipolar couplings are decreased. In some systems, the exponential character of the decay is difficult to be established even for systems with 10 protons. However, the decay constants can still be accurately computed using the method described above. Figure 4 illustrates this point. It shows the magnetization transfer curves computed for a family of systems where the C–C dipolar coupling has been scaled by factors ranging from 1 to 1/128, while the rest of the Hamiltonian was left unchanged. The system chosen for this example is the same as the 10-proton case of Fig. 1. As we know from theory (Eq. (49)), the decay constant is proportional to the square of the dipolar coupling between the carbon nuclei. Fig. 4(b) plots the ratios of the decay constants estimated (as described above) from the curves in Fig. 4(a) to the decay constant estimated for the curve with no scaling. One can see that the decay constants scale exactly as the square of the scaling factor. The rms of the relative deviations of the estimated decay constants from the ideal values determined by the scaling is 0.3% in this case. This suggests that such initial-rate estimates of the spin diffusion constants are very accurate even for the exchange curves that do not look exponential overall.

When we simulated magnetization exchange in similar systems containing three ^{13}C nuclei, the exchange curves exhibited the expected exponential character, in the sense that

$$\mathbf{M}_z(t) = e^{\mathbf{W}t}\mathbf{M}_z(0), \tag{73}$$

subject to the same limitations as seen in the two-spin systems above. The spin diffusion rate constants composing the rate matrix $\mathbf{W}$ were in close agreement with the constants computed for individual spin pairs in the same system, in full agreement with the multi-site exchange theory formulated above. Thus, it appears that the multi-site spin diffusion can be simulated in two steps. First, one obtains the spin diffusion rate constants independently for each pair of ^{13}C nuclei as described above (via full quantum-mechanical dynamics simulations). Second, one uses these constants to build the spin diffusion rate matrix, and then simulates the exchange in the actual experiment via the master equation. We refer to this

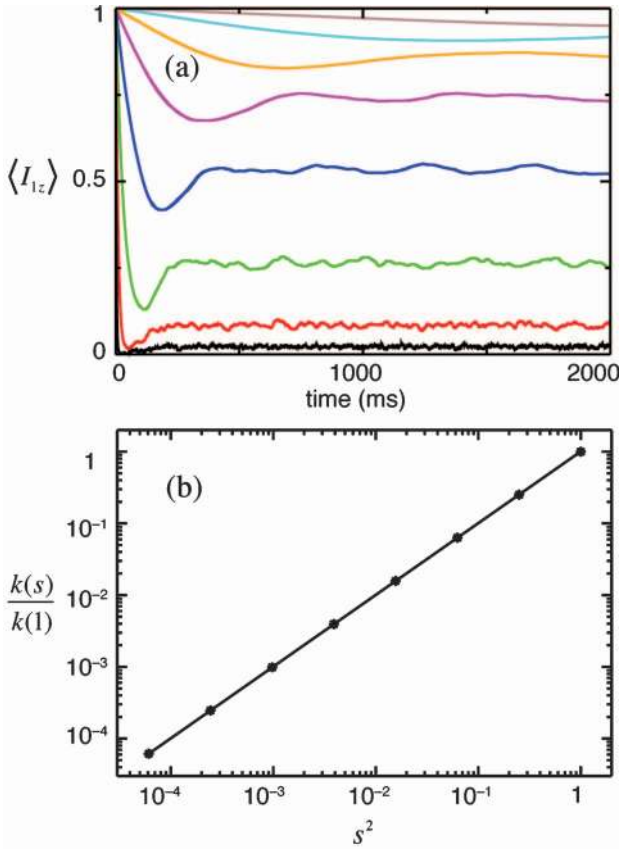

FIG. 4. The effect of scaling of the C–C dipolar coupling on the magnetization exchange between C_α and C_β in serine during R^3-PDSD. Long-term $\langle I_{1z} \rangle$ behavior (a) for the dipolar coupling scaling factor s of 1 (black), 1/2 (red), 1/4 (green), 1/8 (blue), 1/16 (magenta), 1/32 (orange), 1/64 (cyan), and 1/128 (brown). Double logarithmic plot (b) of the PDSD decay constants estimated from the curves shown in (a); the decay constants are plotted as ratios to the decay constant for estimated for $s = 1$. The spin system is the same as the 10-proton system in Fig. 1; other conditions are the same as in Fig. 1. The solid line in (b) is the best-fit straight line through the data.

as the "hybrid" method since it combines the reversible and irreversible dynamic models.

IV. EXPERIMENTAL METHODS

A. NMR samples

Uniformly-[^{13}C,^{15}N]-labeled L-serine was purchased from Cambridge Isotopes (Andover, MA), diluted to 10% in the natural abundance serine and crystallized from water. Selectively labeled Gly-Gly-Val dihydrate (GGV) and Ala-Gly-Gly monohydrate (AGG) samples (kindly provided by Marvin Bayro) were prepared by solid-phase synthesis as described in Ref. 54. The peptides were labeled as [^{15}N]Ala-[1,2–$^{13}C_2$, ^{15}N]Gly-[1–^{13}C, ^{15}N]Gly and [1–^{13}C, ^{15}N]Gly-[2–^{13}C, ^{15}N]Gly-[1–^{13}C, ^{15}N]Val. GGV was diluted in the natural abundance peptide to 8.5%, and AGG to 8%.

B. NMR experiments

NMR spectra were recorded at 11.75 T (125 MHz ^{13}C) using a 4 mm Chemagnetics probe and custom-designed spectrometer and data acquisition and processing software courtesy of Dr. David Ruben. Polycrystalline samples of serine, GGV, and AGG were packed in the center third of the rotor to reduce the inhomogeneity of the RF field to ~5%. The sample spinning frequency was controlled by a Bruker controller and was stable to within a 1–3 Hz. A recycle delay of 3 s was used in all cases. The pulse sequence of the 2D R^3-PDSD experiment is shown in Fig. 5. TPPM decoupling with the field of ~105 kHz was used during the t_1 and t_2 evolution periods and was optimized to yield the narrowest lines, which included optimization of the ^{1}H RF frequency. The same ^{1}H RF frequency was used during the PDSD period. Ramped CP was optimized for overall signal amplitude. The indirect dimension was sampled with the rate of one point per four rotor periods and the dimension size of 64 points. Axial peak suppression was achieved by cycling the phase of the CP lock (as 0° and 180°) on top of the standard 8-step solid-state phase cycle consisting of CYCLOPS and the CP temperature sign cycles. Hypercomplex method[55] was used for frequency discrimination in the indirect dimension. The three diagonal and six cross peaks were integrated for each sample by summing the amplitudes of all points within the peak area using MATLAB.

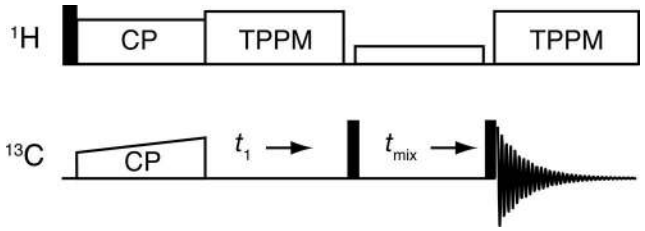

FIG. 5. The pulse sequence of a 2D R^3-PDSD experiment. A CW RF field with $\omega_{RF} = \omega_R$ is applied at ^{1}H frequency during PDSD.

C. X-ray crystallography

The structures of GGV and AGG were determined by Dr. Peter Müller at the MIT Department of Chemistry X-Ray Diffraction Facility. The peptides (purchased from Bachem) were crystallized from water at room temperature by slow evaporation. Low temperature diffraction data were collected on a Siemens Platform three-circle diffractometer coupled to a Bruker-AXS Smart Apex CCD detector with graphite-monochromated Mo Kα radiation (λ = 0.71073 Å), performing φ- and ω-scans. The diffractometer was equipped with a Cryo Stream 700 by Oxford Cryosystems, and a complete data set to a very high MoO was collected at 100 K. The structure was solved by direct methods using SHELXS[56] and refined against F^2 on all data by full-matrix least squares with SHELXL-97. All X–H bond distances in the refined structure were set to the standard target values. Resulting crystal structures are available as structure 06183/himp (AGG) and structure 06126/himp (GGV) on Reciprocal Net (http://reciprocal.mit.edu/recipnet/index.jsp).

V. SIMULATION METHODS

The data obtained in the R^3-PDSD experiments described above were simulated in two stages. In the first stage, we

computed the spin diffusion rate constants for all relevant ^{13}C spin pairs in serine, AGG, and GGV for 100 orientations of the crystallite in the MAS rotor. The orientations were defined through the (α, β) Euler angle pairs of the REPULSION-100[57] set for spherical integration. The third angle, γ, which defines rotation around the rotor axis, does not require averaging (cf. Fig. 3). In the second stage, the constants were used to set up the spin diffusion rate matrix $\mathbf{W}$ for each crystal orientation, which was then used to compute the spin diffusion (followed by the averaging over the orientations). The details of these simulations are explained in the rest of the section. The spin systems and corresponding spin diffusion rate matrices for Eq. (78) were generated in MATLAB. All other computations were performed using SPINEVOLUTION[37] in single precision arithmetic. The typical input files for the simulations will be included in the set of examples distributed with the program in its future releases.

A. Computation of the spin diffusion rate constants

Two independent methods were used to compute the spin diffusion constants: direct and through the zero-quantum lineshape. In the direct method, the equation of motion for the time evolution operator was numerically integrated with the Hamiltonian given by Eq. (2) over one rotor cycle. The parameters of the Hamiltonian were chosen as explained below. The integration was performed by the exponentiation of the Hamiltonian via the Chebyshev expansion, in steps of 3 μs. The resulting propagator was used to propagate the density matrix for 16 rotor cycles if the ^{13}C pair was directly bonded, and for 64 rotor cycles in all other pairs. The initial state was I_{1z}, while I_{2z} was the observable. The spin diffusion constant for the given crystal orientation was computed as

$$w_{ij} = \frac{-\ln(1-2s)}{2t}, \tag{74}$$

where t is the evolution time equal to $16\tau_R$ or $64\tau_R$ and the signal s is defined as in Eq. (56).

In the spectral densities method, we used the expression for the decay constant given by Eq. (50). The spectral densities were computed through the numerical simulation of the zero-quantum coherence decay with the help of a modified g-COMPUTE algorithm.[58] The same Hamiltonian was used as with the direct method, except for the C–C dipolar coupling and the ^{13}C isotropic chemical shifts, which were taken into account explicitly through Eq. (50). The integration of the equation of motion for the propagator was performed by the exponentiation of the Hamiltonian via the Chebyshev expansion, in steps of 3 μs. The initial density matrix was $I_1^+ I_2^-$, and the observable was $I_1^- I_2^+$. The signal was acquired with 2^{16} points sampled every 5 μs. Gaussian apodization with 500 Hz line broadening was applied to the signal before FFT.

To evaluate the agreement between two sets of spin diffusion constants computed with two different methods (or variations of the same method), we used the relative discrepancy, defined as

$$\varepsilon_{ij}^{\mathrm{AB}} = \frac{(w_{ij}^{\mathrm{A}} - w_{ij}^{\mathrm{B}})}{w_{ij}^{\mathrm{A}}}, \tag{75}$$

and characterized by its mean and standard deviation over the set of orientations for which the constants were computed. If one of the methods is known to produce accurate results, then these parameters measure the error in the constants produced with the other method. Note that the sign and the magnitude of the mean $\varepsilon_{ij}^{\mathrm{AB}}$ quantify the degree to which the methods overestimate or underestimate the constants for the given pair of spins.

B. Simulation of the experimental data

Assuming that the exchange is strictly intramolecular, and only labeled sites are involved, the experimental peak intensities $\mathbf{S}(t)$ are related to the powder averaged magnetization exchange curves $\bar{\mathbf{s}}(t)$ computed from Eq. (72) by the following equation:

$$S_{ij}(t) = f_i q_j (\bar{s}_{ij}(t) + \delta_{ij} x_{NA} \exp(-R_i t)). \tag{76}$$

Here, $S_{ij}(t)$ is the integral intensity of the peak appearing at the frequency of spin i in the indirect dimension, and spin j in the direct dimension, after a spin diffusion period of duration t. $x_{NA}\exp(-R_i t)$ are the contributions to the diagonal peak intensities arising from the natural abundance material. The factors f_i and q_j account for the overall normalization of the signal, the small differences in the initial polarizations of the ^{13}C spins resulting from non-uniform cross-polarization, the signal lost in the sidebands, and the variations in the peak lineshapes. The relaxation rates and the scaling factors are unknown and hence were obtained by fitting Eq. (76) to the experimental data. As only five of the scaling factors are independent, $q_1 = 1$ was used as a fixed value. In the case of serine, all relaxation rates were assumed to be zero, as relaxation is too slow on the time scale of the spin diffusion in this system.

Equation (76) is an idealization, as it does not account for the exchange of magnetization with the neighboring labeled molecules, as well as with the natural abundance ^{13}C nuclei. These effects are particularly large in the AGG and GGV samples due to the relatively long distances over which the intramolecular exchange is occurring in these samples, with the longest distance of ~4.9 Å in either case. For example, on average, for one labeled GGV molecule, within 7 Å of its labeled nuclei, there are 1.3 intermolecular contacts to other labeled molecules, and 1.1 contacts to the natural abundance ^{13}C nuclei. This means that most of the labeled molecules in the crystal are coupled to each other, forming a random network that spreads throughout the entire crystal. The only way to account for these contacts is through the explicit simulation of spin diffusion in small crystallites set up to imitate the distribution of the labeled molecules and natural abundance nuclei in the actual sample. The following procedure was used to accomplish this.

The crystallite sizes of $7 \times 7 \times 7$ unit cells were used for serine and GGV, and $9 \times 9 \times 9$ unit cells for AGG. The spin systems formed by the ^{13}C nuclei appearing in such crystallites contained from 230 to 450 spins. Crystallites with smaller dimensions yielded unacceptably large fluctuations in the results. The surface effects were eliminated through the use of the periodic boundary conditions, i.e., the spin

diffusion rate matrix **W** for the crystallite was computed assuming that the spin system was periodically replicated along all three crystallographic axes. As the model allows a choice of the purity of the ^{13}C labeling, we used the 99% purity for each labeled site in all three compounds. The labeled molecules, the ^{12}C impurities in them, and the natural abundance ^{13}C nuclei in the crystallite were randomly chosen for each orientation used for the orientational averaging. To simplify the computation of the spin diffusion rate matrices for systems of this size, the intermolecular spin diffusion constants were not computed directly but rather estimated from the corresponding intramolecular constants by appropriately scaling them:

$$w_{ij} = \frac{w_{IJ} r_{IJ}^6}{r_{ij}^6}, \tag{77}$$

where (I, J) is the intramolecular spin pair corresponding to the intermolecular pair (i, j). Since the orientation of the pair (i, j) may be arbitrary, while the orientation of the pair (I, J) is fixed for a given crystallite, this approximation would be unacceptable for the computation of individual spin diffusion constants. However, for the simulation of the orientationally averaged magnetization exchange, the method appeared to yield accurate results. The experimental peak intensities were computed as follows:

$$S_{ij}(t) = N^{-1} f_i q_j \overline{P_i^T \exp(\mathbf{W} - \mathbf{R})t P_j}, \tag{78}$$

where the bar symbolizes orientational averaging, N is the average number of labeled molecules in the crystallite, and P_i is the vector of zeros and ones, with the ones appearing at the spins located at the site i. Note that if the intermolecular exchange is neglected, Eq. (78) becomes equivalent to Eq. (76).

C. Parameters of the Hamiltonian

The dipolar coupling parameters were computed from the atomic coordinates of the nuclei. The coordinates were taken from the x-ray crystallographic structures obtained as described above for GGV and AGG, and from Ref. 59 for serine (each of the structures has one molecule per asymmetric unit). Unless otherwise specified, the spin system was composed of two ^{13}C nuclei and 10 nearest protons from their local environment. The protons were chosen as follows. First, a single molecule was selected in the crystal structure, and the list of all protons within 4.5 Å of the carbon nuclei in this molecule was compiled (the local environment). Then, for each carbon pair of interest, 10 protons were chosen from this list that had the largest values of $1/r_1^3 + 1/r_2^3$, where r_1 and r_2 are the distances to the first and the second carbon nucleus in the pair.

The dipolar coupling for directly bonded ^{13}C–^{13}C and ^{13}C–^{1}H pairs was corrected to account for the vibrational averaging[60] and for the intrinsic inability of the x-ray crystallography to accurately determine bond lengths to proton nuclei.[61] The effective directly bonded C–H distances were set to 1.12 Å (chosen as a consensus value from Refs. 62–65). The directly bonded C–C distances were effectively increased by 0.025 Å, which corresponds to the difference in the effective distance of 1.55 Å measured in Ref. 66 for glycine and the distance of 1.525 Å observed in its structure obtained by diffraction methods.

The ^{13}C CSA values and orientations were taken or estimated from a number of sources.[54,67–74] The ^{13}C isotropic chemical shift values used were taken from the experiment. The ^{1}H chemical shift and CSA values were neglected in most of the computations presented in this work. The notable exception is the computation of the spectral densities for Figs. 9–11: the zero-quantum coherence does not decay completely if the ^{1}H CSA and chemical shifts are neglected at high spinning frequencies and ^{1}H RF fields away from the rotary resonance. For these computations, and in order to investigate the significance of the ^{1}H CSA/CS effects in other situations, the necessary values were estimated from Ref. 75.

All –NH_3 groups, methyl groups, and water molecules were assumed to undergo fast regime three-[76–78] and twofold[79] hopping, respectively, resulting in the appropriate averaging of the related CSA and dipolar coupling tensors. If not all protons of the group participating in the exchange were included in the spin system, the exchange had to be neglected. When computing the spin diffusion constants for the directly bonded CO–CA pair in AGG, all three protons of a nearby –CH_3 group were included in the spin system to account for the fast hopping, even though only two of them were among the 10 closest protons.

The isotropic J-couplings for the directly bonded C–C pairs were assumed to be 35 Hz.

VI. RESULTS AND DISCUSSION

A. R^3-PDSD in serine and peptides

As explained in Sec. V, the experimental data obtained for R^3-PDSD in serine, AGG, and GGV samples were simulated using two different methods for the computation of the spin diffusion constants. Both approaches yeilded very similar results, although the constants obtained with the spectral densities method were slightly larger on average. The typical relative discrepancy between the methods (as defined by Eq. (75)) had a mean of about 0.5%. The directly bonded pairs and the CO–CO pair in AGG were exceptions, exhibiting much larger deviations, with the extreme of 3.8% in the case of CO–CA in serine. The only pair for which the spectral densities method yielded systematically smaller constants (by 1.6%) was CA–CB in serine. The standard deviation of the discrepancy between the two methods was typically around 1%, with the exception of CO–CA in serine, where it was 3.8%. As discussed below, the larger discrepancies observed for the directly bonded pairs is a consequence of the exchange being too fast in these cases, which leads to deviations from the exponential behavior.

The residual sums of squares (RSS's) obtained in fitting Eq. (78) to the experimental data in serine were 15% larger using the constants computed with the spectral densities method than with the direct method. In peptides, the RSS's were nearly the same for the two methods. The difference observed in serine is expected, given the systematic bias in the CO–CA constants mentioned above. The data and

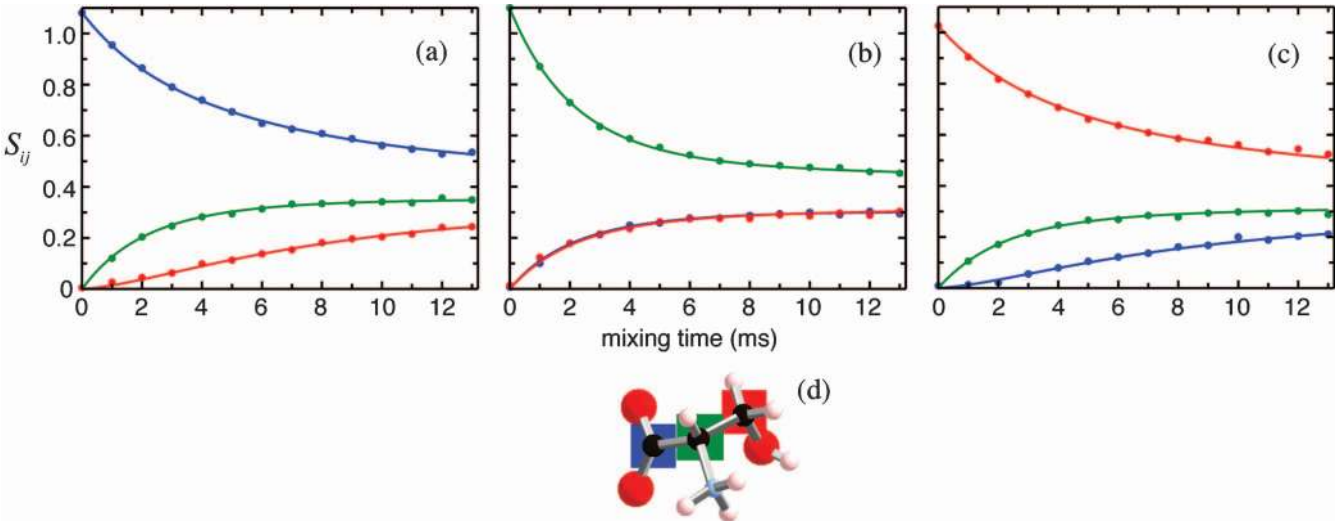

FIG. 6. Intensities of the diagonal and cross peaks in 2D ^{13}C MAS correlation experiments using R^3-PDSD for mixing in U-[^{13}C, ^{15}N]-L-serine (a-c). The spinning frequency and the ^{1}H RF field are 10 kHz. The sample was diluted to 10% by the natural abundance compound. The asterisks represent the data; the solid lines represent the simulations. The ^{13}C–labeled sites are enclosed in colored boxes in (d); the color used for each peak corresponds to the color of the ^{13}C site in the *direct* dimension for the peak.

the results of the simulations are presented in Figs. 6–8. The magnetization exchange curves obtained with the two methods were virtually indistinguishable visually, and we chose to display only one set of curves for each molecule.

The residual errors observed in the data fits can be separated into two main components: one randomly fluctuating from point to point, and the other slowly drifting along the data curves. The first component can be attributed to the

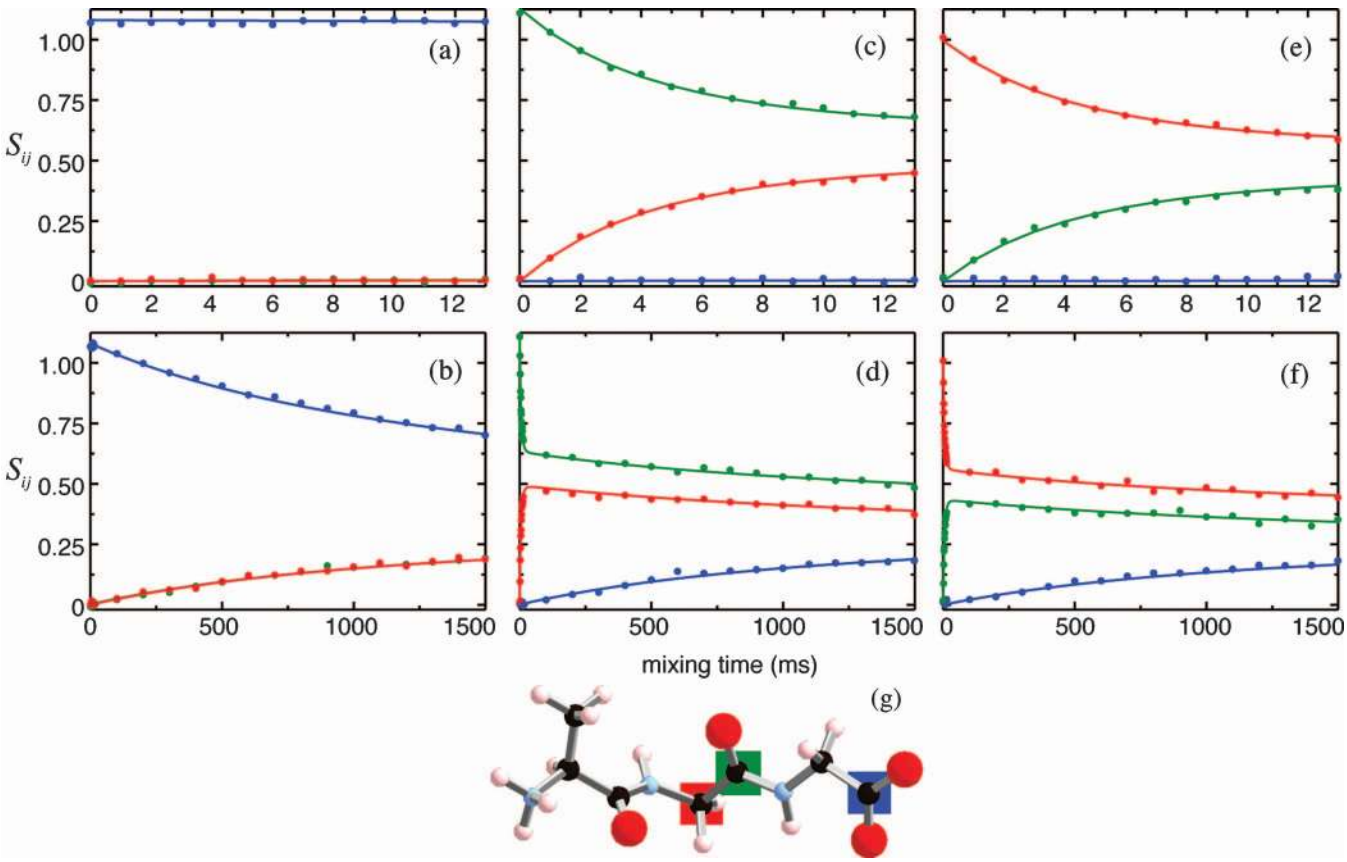

FIG. 7. Intensities of the diagonal and cross peaks in 2D ^{13}C MAS correlation experiments using R^3-PDSD for mixing in a specifically ^{13}C–labeled AGG: the initial evolution up to 13 ms (a,c,e) and the full curves (b,d,f). The spinning frequency and the ^{1}H RF field are 10 kHz. The sample was diluted to 8% by the natural abundance compound. The asterisks represent the data; the solid lines represent the simulations. The ^{13}C–labeled sites are enclosed in colored boxes in (g); the color used for each peak corresponds to the color of the ^{13}C site in the *direct* dimension for the peak.

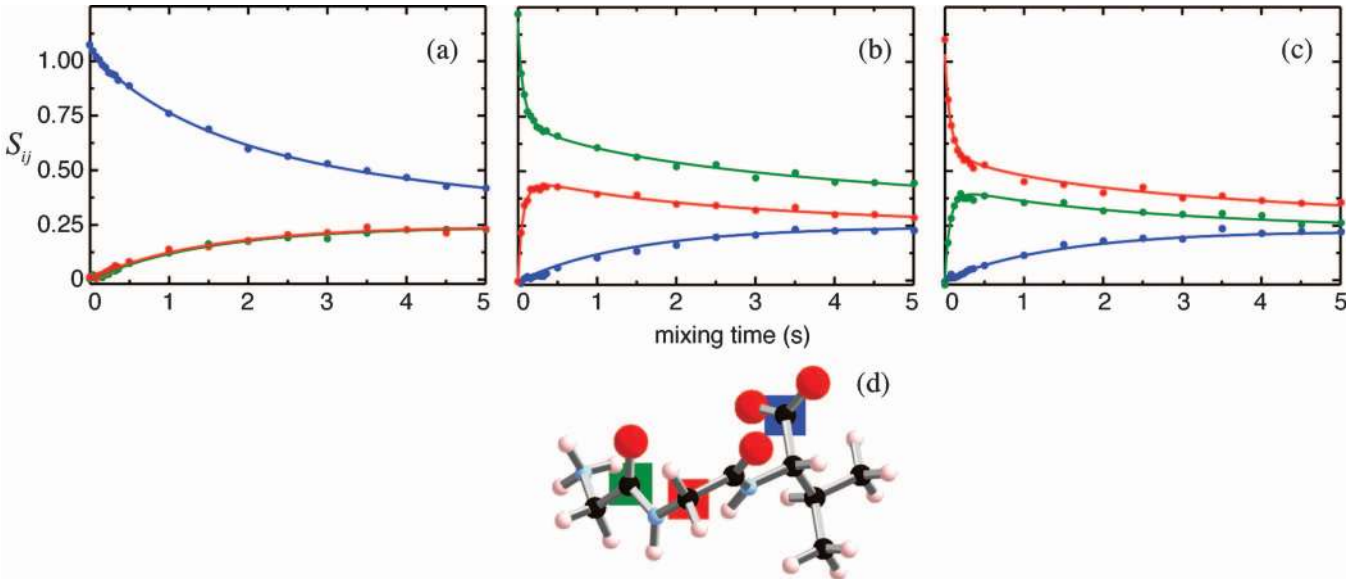

FIG. 8. Intensities of the diagonal and cross peaks in 2D ^{13}C MAS correlation experiments using R^3-PDSD for mixing in a specifically ^{13}C–labeled GGV (a-c). The spinning frequency and the ^{1}H RF field are 10 kHz. The sample was diluted to 8.5% by the natural abundance compound. The asterisks represent the data; the solid lines represent the simulations. The ^{13}C–labeled sites are enclosed in colored boxes in (d); the color used for each peak corresponds to the color of the ^{13}C site in the *direct* dimension for the peak.

random experimental error, while the second – to the error of the model. Such separation can be achieved, for example, by fitting the data to a multi-exponential model of the form

$$\hat{\mathbf{s}}(t) = \sum_i \alpha_i e^{(\mathbf{W}_i - \mathbf{R}_i)t}, \tag{79}$$

using $\hat{\mathbf{s}}(t)$ instead of $\bar{\mathbf{s}}(t)$ in Eq (76), and treating α_i, $\mathbf{W}_i$, $\mathbf{R}_i$, and the scaling factors as the fit parameters. One may assume that for PDSD data, such fits will be able to reproduce all slow changes along the data curves, while leaving the random errors as residuals. We computed these fits using one, two, and three exponentials in Eq. (79). For all three data sets, the residual errors obtained in the three-exponential fits did not exhibit any drifts along the exchange curves and had zero means, thus, appearing completely random. Furthermore, the residual sums of squares obtained using two- and three-exponential fits were relatively similar (thus indicating convergence) in the cases of serine and AGG. Hence, we used the three-exponential RSS's to estimate the rms of the random data error. The differences between these RSS's and the RSS's obtained in fitting the data to the spin diffusion simulations were attributed to the errors of the model. The estimates obtained in this fashion are summarized in Table I. To validate this treatment, we verified that addition of synthetic random noise to the data did not lead to substantial changes in the model error, while causing expected (additive) changes in the random error. The data errors reported in Table I exhibit tendency expected from the signal-to-noise ratio for the samples. Possible sources of the model error are discussed in Sec. VI B.

The RSS of the single-exponential fit to the serine data was 6.3 times larger than the three-exponential fit. When compared with the errors reported for serine in Table I, this clearly demonstrates the non-exponential character of the orientationally averaged magnetization exchange. Characterizing these experimental exchange curves by a single spin diffusion rate matrix, as it has been universally done previously, may lead to large model error.

The relatively small data and model error seen in Table I support the theoretical and computational models proposed in this work and suggest that accurate model parameters may be extracted from the PDSD data. The internuclear distances are, perhaps, the most interesting parameters for the applications. When all other model parameters are known, fitting the distances is straightforward, since the spin diffusion constants scale as r_{ij}^{-6} and thus do not need to be recomputed from scratch for a different set of distances. The random error of such estimates will be proportional to the rms data error, but it will also depend on the specific spin system and the specific set of distances being extracted. The systematic biases in these estimates will be related to the model error and will also depend on the specifics of the system. Three-spin systems will typically be rather unfavorable for accurate determination of their geometry. As an example, in serine, the CO–CB spin diffusion constants are smaller than the constants for the directly bonded pairs by a factor of 20. As a consequence, most of the transfer between CO and CB will be relayed through the CA nucleus, and the data will be relatively insensitive to the CO–CB distance. In AGG, on the other hand, the spin diffusion constant for the directly bonded pair is about 400-fold lager than the other two. As a result, the two directly

TABLE I. The rms error per point estimated for the data and simulations shown in Figs. 6–8.

	Serine	AGG	GGV
σ_D, %[a]	0.54	0.79	1.02
σ_M, %[a]	0.40	0.39	0.73

[a]σ_D is the data error, σ_M is the model error; measured as a fraction of the initial signal, i.e., of a diagonal peak intensity at $t_{mix} = 0$.

TABLE II. The internuclear distances obtained by fitting the data.

	Serine			AGG			GGV		
r_{ij}[a]	r_0[b]	$\hat{r}/r_0$	CI,[c]%	r_0[b]	$\hat{r}/r_0$	CI,[c]%	r_0[b]	$\hat{r}/r_0$	CI,[c]%
r_{12}	1.552	0.9976	±0.22	3.712	1.011	±0.46	4.91	1.0058	±2.3
r_{13}	2.526	0.9952[d]	±1.5	4.873	1.021	±1.1	4.53	0.9986	±0.68
r_{23}	1.535	0.9978	±0.23	1.555	0.994	±0.29	2.41	0.9959	±0.61

[a]The ^{13}C nuclei are numbered as follows: CO (1), CA (2), CB (3) in serine; Gly-3 CO (1), Gly-2 CO (2), Gly-2 CA (3) in AGG; Val-3 CO (1), Gly-1 CO (2), Gly-2 CA (3) in GGV.
[b]The effective internuclear distance computed from the x-ray crystal structures and corrected for the vibrational averaging for directly bonded pairs (by +0.025 Å (Ref. 66)).
[c]The 95% confidence intervals estimated assuming identically and independently distributed Gaussian errors.
[d]Computed using $r_{12}/r_{12(0)} = r_{23}/r_{23(0)} = 0.9978$.

bonded nuclei will behave essentially as one on the time scale of the exchange with the remote nucleus, and the data will be insensitive to the individual values of the two weaker constants, depending mostly on their sum. Fortunately, in uniformly labeled proteins or other large molecules, such ambiguities in individual internuclear distances will typically be compensated by the purely geometric constraints.

Without such constraints, simultaneous fitting of all distances is likely to produce large errors due to the effects mentioned above. With the three-spin systems used in the present work, fitting the distances one at a time, while using the known values for the other two, is the best one can do to characterize the potential of the method, even though the intention is to fit all the distances simultaneously in the applications. Table II summarizes the results of such data fits computed using Eq. (78). As one can see, most of the distance estimates are both very accurate and precise. The relatively large errors in the CO–CB distance in serine and the two longer distances in AGG are in agreement with our remarks above. The large error bar on the CO–CO distance in GGV is due to a similar effect. The impact of the lack of constraints in AGG on the distance estimates can be illustrated by optimizing r_{13} while having the value of $r_{12}/r_{12(0)}$ fixed at 1.01. This results in $\hat{r}_{13}$ value being off by only 0.06%, in contrast to the 2.1% error reported in Table II, which was obtained for $r_{12}/r_{12(0)} = 1$. As mentioned above, we expect that in larger systems such uncertainties in the distance estimates will be much less problematic since one will fit the internal molecular coordinates rather than distances in these situations. Furthermore, this issue can be significantly alleviated through the use of two or more PDSD data sets for the same molecule (obtained with different ^{1}H RF fields and spinning frequencies), especially if they are designed to provide complementary information.

B. Factors affecting the accuracy

The coupling of ^{13}C nuclei to the directly bonded protons (or equivalent effective distance) is the primary factor determining the shape of the spectral density functions, and thus will strongly affect the spin diffusion constants. However, due the vibrational averaging effect,[60] it cannot be determined directly by the diffraction methods, and there is a considerable disagreement in the literature regarding its exact value.[62–65,80] In the present work, we used the effective C–H distance of 1.12 Å to compute these couplings in all CH and CH_2 groups, but it is likely that using different (and more accurate) values for different groups could improve the accuracy of the simulations in the future. Independent PDSD experiments can be readily designed to measure these couplings very accurately. For example, from the dependence of the serine CO–CA spin diffusion constants on the effective C–H distance in the CA group, we estimate that the 1.12 Å value should be accurate to within ±0.007 Å for this group.

The vibrational averaging of the directly bonded C–C dipolar couplings is just as important. Accurately measured by the diffraction methods, the distances between directly bonded sp^3 hybridized carbons exhibit a significant variation in various compounds. In order to account for vibrational averaging, we used a uniform correction of +0.025 Å for these experimental values, which follows from the effective C–C distance in glycine[66] and the assumption that this correction is approximately the same for all C–C pairs in question. For future work, this correction can be determined even more accurately from our serine data. Indeed, in contrast to the CO–CA spin diffusion constants, the CA–CB constants in serine are unaffected by small variations in the effective C–H distance and thus are independent on our assumptions regarding the value of this parameter. Since all other parameters of the serine model are relatively reliable, the estimate for the effective CA–CB distance in serine of 1.532 ± 0.0035 Å given in Table II appears to be the most accurate estimate of a dipolar coupling in a directly bonded C–C pair available to date. Using this estimate, and taking 1.514 ± 0.002 Å as the CA–CB distance given by the diffraction methods,[81] we can estimate that the vibrational averaging correction should be +0.018 ± 0.004 Å (at room temperature).

The CSA values and orientations may introduce considerable amount of uncertainty in the results of the simulations. For the peptides used in this work, most of these parameters were estimated from the known values in similar compounds, while the tensor orientations assumed for the C_α nuclei were essentially arbitrary. Nevertheless, this should not present a fundamental problem when simulating PDSD in proteins, since in that case the ^{13}C CSA parameters are accessible through *ab initio* calculations,[82] or can be estimated from the isotropic chemical shift values.[83]

The exchange of the protons in the nearby $–NH_3$ and $–CH_3$ groups should also be taken into account in the simulations. Freezing this exchange in the serine, for example, leads to noticeable overestimation of the constants, with the largest relative errors observed for the CO–CA pair (2% mean and 9% standard deviation).

The limited number of protons that can be included in the simulations is also a potential source of error in the computed constants. Nevertheless, in most cases we observed in the simulations, the values computed for the spin diffusion constants essentially converged by the tenth proton added to the system and exhibited little dependence on the exact set of protons included, as soon as the most proximate protons were in the set. The relative discrepancies observed in such simulations typically had standard deviations on the order of 1%, but

their means were much smaller. Including only eight protons tended to result in lower accuracy.

The ^{13}C longitudinal relaxation rates were assumed isotropic in this work and were treated as fit parameters as explained above. The values obtained in the fits ranged from 0.02 to 0.06 s^{-1}. Two exceptional values were obtained in AGG, one of which was nearly zero and the other negative. These unphysical values were possibly compensating for a systematic error in the data and were allowed by the insufficiently long time during which the exchange was observed in this sytem. The assumption of the longitudinal relaxation being isotropic is clearly a rough approximation. While it was acceptable for fitting the AGG data, its contribution to the much larger model error in the case of GGV may be significant. The dynamic exchange of protons in the $–NH_3$ and $–CH_3$ groups and water molecules constitutes a major source of the ^{13}C longitudinal relaxation in biomolecules, which is not difficult to compute theoretically. Such computations can be used in the future to estimate the anisotropic parts of the relaxation rates. We expect that this will be particularly important if the ^{13}C nuclei of the $–CH_3$ groups participate in the spin diffusion, as the longitudinal relaxation on these nuclei is very fast and they will act as maznetization sinks in the course of the exchange.

As observed for the CO–CA pair in serine, the deviations from the exponential character of the exchange dynamics can become significant due to the exchange being too fast to neglect on the timescale of the correlation time τ_c. In such cases, prior to reaching a stationary value, the spin diffusion constant is time-dependent during an initial period of duration τ_c (see Fig. 3). The direct method gives better data fits as it computes an average value, while the spectral densities method produces the extreme stationary value. For higher accuracy of the simulations, one may possibly use time-dependent spin diffusion constants obtained with the direct method, or rely on the non-Markovian equation (34) to compute the exchange curves.

As explained in Sec. V, accounting for the intermolecular magnetization exchange, as well as for the exchange with natural abundance ^{13}C nuclei is essential for accurate simulation of the data. Neglecting these effects, for example, in GGV, leads to the estimate of the CO–CO distance that is off by about 10% from the correct value, in contrast to only 0.6% error seen in Table II. The procedure we used to compute the spin diffusion rate matrix for Eq. (78) is somewhat crude and may also serve as a potential source of error (the intermolecular spin diffusion constants were estimated from the intramolecular constants). In addition, while for serine we used individually computed spin diffusion constants for all four molecules in the primitive unit cell, for AGG and GGV, we used only one set of constants, even though these compounds have two molecules per primitive unit cell.

The powder averaging scheme (REPULSION-100[57]) and the integration step (3 μs) we chose for this work may also have compromised the accuracy of some of our computations. This choice was made at the early stages of the work and was influenced by the lack of the available computational resources at the time. For the future applications, hemispherical nodal sets appear to be more efficient than spherical sets for orientational averaging, but we have not explored this issue in detail.

The effects of the ^1H chemical shifts and CSAs on the spin diffusion constants in our model compounds were quite small. The discrepancies between the sets of constants computed with and without these terms in the Hamiltonian were typically well under 1% in mean and under 3% in the standard deviation. Thus, they are unlikely to be significant for practical purposes, and we chose to neglect them altogether.

C. PDSD via spectral densities

In the expression for the PDSD constant, Eq. (49), the effects of the C–C dipolar coupling and of the ^{13}C isotropic chemical shifts and CSA tensors are described analytically. The effects of all other parameters of the Hamiltonian, namely, the C–H and H–H dipolar coupling terms, the RF field, and the spinning frequency, are accounted for through the spectral density function, which is computed numerically as the zero-quantum coherence decay lineshape. Note that we define the zero-quantum lineshape as purely dipolar in the sense that it does not contain the effects of the ^{13}C chemical shift (although it does contain the effects of the ^1H chemical shift, if present). This is different from the use of the term by most other authors who follow Kubo and McDowell.[36] Our definition is preferred because it results in very similar lineshapes for the pairs of spins of the same type (e.g., CO–CH).

Owing to the sample rotation, the spectral density is expressed as a set of Fourier components $J_k(\omega)$. In general, all of these components must be taken into account in the computations. However, for qualitative insights, it is often sufficient to consider only the $k = 0$ component. It is typically the largest in magnitude, and its integral is equal to one, as follows from the normalization of $G(t;\tau)$. Due to the symmetry expressed by Eq. (55), the real part of $J_0(\omega)$ is approximately even, while the imaginary part is approximately odd. The specific shape of the spectral density depends on the combination of the three main factors: the spin system, the ^1H RF field, and the spinning frequency. In Fig. 9, we show the orientationally averaged $J_0(\omega)$ for three kinds of ^{13}C pairs: CO–CO, CO–CH_2, and CH_2–CH, computed for the spinning frequencies of 10 and 50 kHz and various ^1H RF field amplitudes (using a CW field). One can see that the rotary-resonant RF fields (with $\omega_{RF} = \omega_R$) result in spectral densities characterized by a single central peak with a width given (qualitatively) by the overall strength of the C–H dipolar couplings in the system. Other conditions result in the spectral densities containing bands at $n\omega_R$ and $n\omega_R \pm \omega_{RF}$ (for high spinning frequencies), or exhibiting more complex band patterns. Although it is generally assumed that the zero-quantum lineshapes are Lorentzian (e.g., when accounting for relaxation in rotational resonance experiments), the simulations show that this is probably never the case. For example, the bell-shaped lines corresponding to rotary-resonant conditions in Figs. 9(a) and 9(b) and E are actually much closer to Gaussian than to Lorentzian. Furthermore, under the conditions typical for high-power CW decoupling, the CO–CO zero-quantum

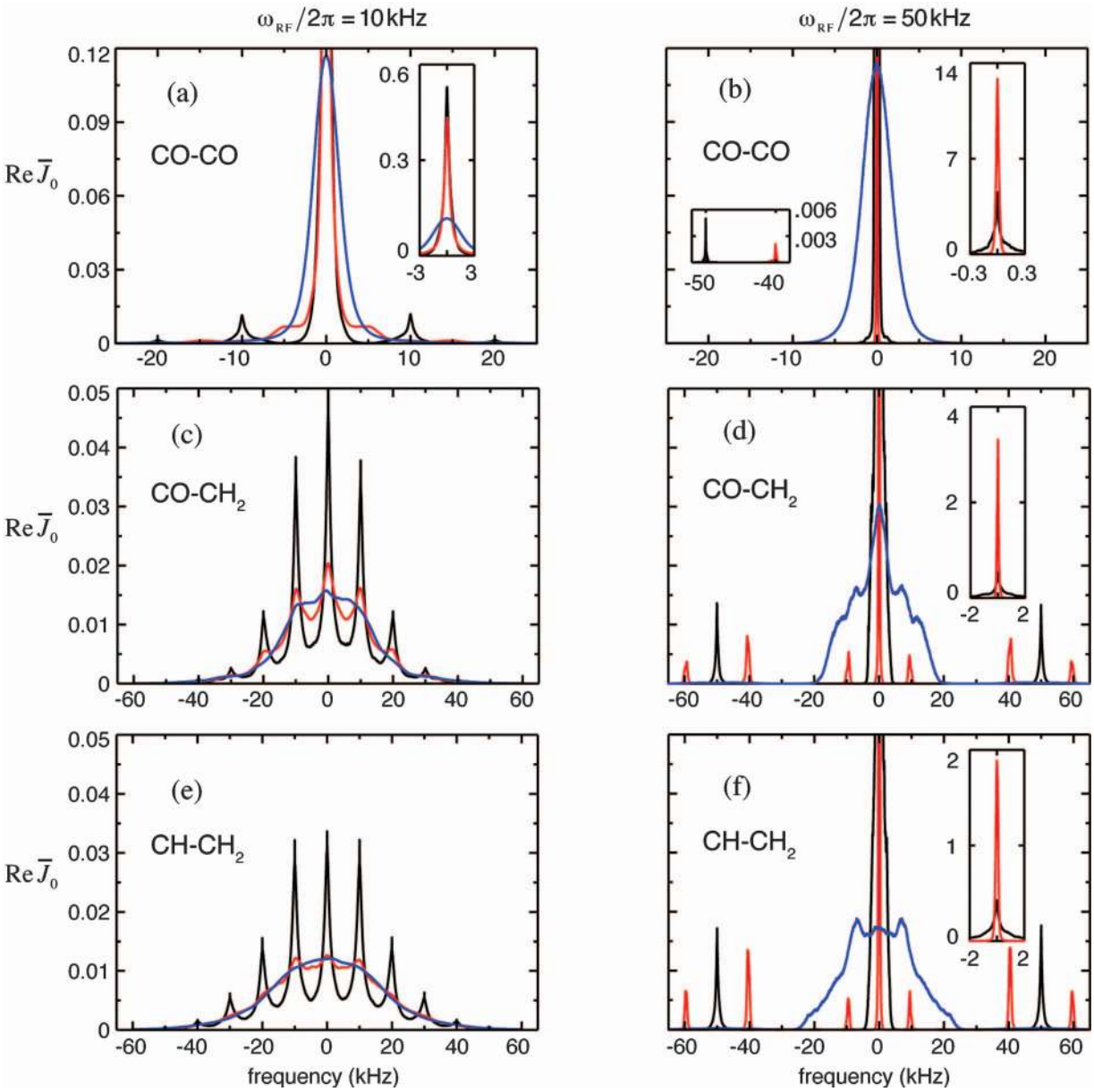

FIG. 9. Orientationally averaged real components of the spectral densities $J_0(\omega)$ for representative ^{13}C pairs in GGV: {Gly1–CO, Val3–CO} (a and b), {Gly1–CO, Gly2-CA} (c and d), {Gly2-CA, Val3-CA} (e and f) computed for spinning frequencies of 10 kHz (a,c,e) and 50 kHz (b,d,f). At the spinning frequency of 10 kHz, the ^{1}H RF field amplitudes are 0 (black), 5 (red), and 10 (blue) kHz. At the spinning frequency of 50 kHz, the ^{1}H-resonant RF field amplitudes are 0 (black), 10 (red), and 50 (blue) kHz.

lineshape approaches a nearly ideal Gaussian. The sidebands appearing at $n\omega_{\mathrm{R}} \pm \omega_{\mathrm{RF}}$ (Figs. 9(b), 9(d), and 9(f)) correspond to the MIRROR recoupling conditions,[29] which suggests that the magnetization exchange observed under these conditions is a special case of PDSD and, thus, can be naturally explained and quantitatively simulated using the methodology developed in the present work.

Various qualitative insights can be drawn from these figures in conjunction with Eq. (49). As an example, one can observe that the CO–CO spectral densities consist of single narrow peak, except for the no-RF case, which exhibits small sidebands at $\omega = \pm\omega_R$. Considering that the isotropic chemical shift difference in CO–CO pairs is very small, this restricts the summation indices in Eq. (49) to $n = 0$. In addition, considering that $J_0(\omega)$ is at least two orders of magnitude larger than the other components of the spectral densities for CO–CO pairs (because the proton environment in such pairs is fairly isotropic), one obtains another selection rule, $k = 0$. With these selection rules, Eq. (49) is transformed to

$$k_D^{\mathrm{CO-CO}} = \frac{1}{6}\left|\sum_{k=-2}^{2} D_{2,0}^{(-k)} C^{(k)}\right|^2 \mathrm{Re}\, J_0\left(\omega_\Delta^{\mathrm{iso}}\right). \qquad (80)$$

Since $D_{2,0}^{(0)} = 0$, the spin diffusion constant for a CO–CO pair is determined by the intensities of the $k = \pm 1, \pm 2$ sidebands of the CSA difference for the nuclei. This implies, for example, that in α-helices and β-sheets in proteins, the PDSD constants for many carbonyl pairs will be heavily attenuated due to the relative similarity of their CSA tensors resulting from the high degree of alignment of the CO groups. This also

implies that the accuracy of the computed spin diffusion constants for CO–CO pairs will depend greatly on the accuracy of the CSA parameters used to compute them.

For ^{13}C pairs characterized by similar isotropic chemical shifts and small CSAs, such as CA–CA pairs, the main contribution to the spin diffusion constant will come from the spectral density values around $\omega = \pm\omega_R, \pm 2\omega_R$, entailing that the no-RF PDSD transfer will be more efficient than R^3-PDSD since no-RF spectral densities are distributed mostly at the sidebands. In general, it is clear that various combinations of spinning frequencies and ^{1}H RF fields can be used to design PDSD experiments capable of providing complimentary sets of structural constraints when applied to the same molecule of interest, such as a protein, with the potential of resulting in highly accurate structures.

D. Diffusion in the non-Markovian regime

At high spinning frequencies (Fig. 9) or high ^{1}H RF field amplitudes (e.g., during proton decoupling), the spectral density collapses to a narrow peak at $\omega = 0$, possibly accompanied by a few small sidebands (unless the ^{1}H RF field amplitude matches a rotary resonance condition). This implies comparatively long decay times for the correlation function and may lead to the breakdown of the conditions required for the spin diffusion dynamics to be Markovian. As can be seen from the expression for the spin diffusion constant (Eq. (49)), this breakdown becomes most apparent when $\omega_\Delta^{\text{iso}} = n\omega_R$, where $n = \pm 1, \pm 2$ for small CSAs, or $n = 0, \pm 1, \pm 2, \ldots$ for large CSAs. The exchange of magnetization under these conditions is commonly known as rotational resonance (R^2).[52,53,84] In an isolated two -spin system, this exchange can be represented as precession of the density matrix about the effective Hamiltonian in the (23) spin subspace[46,85] (Eqs. (8)–(10)). However, under typical experimental conditions, this picture is often a poor approximation, as the interactions with protons are rarely negligible even at very high ^{1}H decoupling fields. It has been assumed[46,86] that the effects of these interactions can be described by the zero-quantum relaxation coefficients phenomenologically introduced into the equation of motion of the density matrix for the isolated two-spin system. This assumption postulates a Lorentzian lineshape for the zero-quantum coherence decay (as it operates with the zero-quantum relaxation times T_2^{ZQ}). As we have seen above, these lineshapes are never Lorentzian. Therefore, it should be expected that the standard treatment of rotational resonance is likely to carry a significant model error that has not been previously recognized. The PDSD theory presented above contains rotational resonance as a special, although extreme case, and may constitute a more accurate alternative to the standard semi-phenomenological treatment of R^2. An exploration of this possibility, as well as a test of the validity of the non-Markovian equation (34) is presented below.

If the zero-quantum coherence decay is fast relative to the C–C dipolar coupling strength, R^2 exchange proceeds in the Markovian regime, i.e., as an exponential decay with the constant given by Eq. (49). For the hypothetical case of a Lorentzian zero-quantum lineshape, the expression for the decay constant agrees with the result obtained in Eq. (81).[46] Indeed, at the exact resonance ($\omega_\Delta^{\text{iso}} = n\omega_R$ with $n = 1, 2$), assuming that $J_0(\omega)$ is Lorentzian and neglecting all other $J_k(\omega)$ components and the non-resonant terms, Eq. (49) is transformed to

$$k_D = \left|\omega_D^{(n)}\right|^2 T_2^{ZQ}, \tag{81}$$

which is identical to the expression given in Ref. 46. However, in real systems, Eq. (49) should be generally more accurate than Eq. (81) for the reasons explained above.

In the general case, R^2 exchange should obey the non-Markovian equation (34), which can be solved under assumptions that are significantly milder than the Markovian limit. To arrive at this solution, we first write Eq. (34) in terms of the Fourier components of the correlation function. These components are made obvious by writing the correlation function (Eq. (47)) as follows:

$$\begin{aligned}\Phi(t;\tau) &= \sum_m e^{im\omega_R t}\Phi_m(\tau) + \text{c.c.} \\ &= \sum_m e^{im\omega_R t}\left(\Phi_m(\tau) + \Phi_{-m}^*(\tau)\right),\end{aligned} \tag{82}$$

where

$$\Phi_m(\tau) = \frac{1}{2}\sum_{k,n}\omega_D^{(n)}\omega_D^{(n+k-m)*}e^{-i(\omega_\Delta^{\text{iso}} - n\omega_R + m\omega_R)\tau}G_k(\tau). \tag{83}$$

With this expansion, Eq. (34) becomes

$$\frac{d}{dt}s(t) = -\sum_m e^{im\omega_R t}\int_0^t \left(\Phi_m(\tau) + \Phi_{-m}^*(\tau)\right)s(t-\tau)\,d\tau. \tag{84}$$

The integrals on the right-hand side of Eq. (84) are now convolutions, and this equation can be readily transformed to the frequency domain using the convolution theorem. Applying the Fourier transform to both sides of Eq. (84) results in

$$i\omega S(\omega) - 1 = -\sum_m k_D^{(m)}(\omega)S(\omega - m\omega_R), \tag{85}$$

where

$$k_D^{(m)}(\omega) = K^{(m)}(\omega) + K^{(-m)*}(-\omega), \tag{86a}$$

$$K^{(m)}(\omega) = \frac{1}{2}\sum_{k,n}\omega_D^{(n)}\omega_D^{(n+k-m)*}J_k\left(\omega + \omega_\Delta^{\text{iso}} - n\omega_R\right). \tag{86b}$$

Equation (85) can be "resolved" with respect to $S(\omega)$ as follows:

$$S(\omega) = \frac{1 - \sum_{m\neq 0}k_D^{(m)}(\omega)S(\omega - m\omega_R)}{k_D^{(0)}(\omega) + i\omega}. \tag{87}$$

For a wide range of conditions, the solution to this equation can be approximated as

$$S(\omega) = \frac{1}{k_D^{(0)}(\omega) + i\omega}, \tag{88}$$

while the effects of the terms neglected on the right-hand side of Eq. (87) will be mostly in the sidebands in $S(\omega)$. This is most easily seen in the Markovian regime (cf. Eq. (36)). The

accuracy of the solution given by Eq. (88) can be evaluated by substituting it back to Eq. (87), and more accurate solutions can then be found by iteration. If one is not interested in the small oscillations of $s(t)$ within a rotor cycle (e.g., as seen in Fig. 3), Eq. (88) becomes an acceptable approximate solution.

Equation (88) implies that $S(\omega)$ is Lorentzian if it is sufficiently narrow, i.e., if the decay of $s(t)$ is relatively slow. More precisely, this occurs when $k_D^{(0)}(\omega)$ is approximately constant in the vicinity of $\omega = 0$ for a frequency range much larger than its magnitude. The expression for the decay constant corresponding to this Lorentzian is exactly the same as given by Eq. (49), i.e., $k_D = k_D^{(0)}(0)$, but now we obtained it under less stringent conditions, which are also more readily accessible for direct verification.

Just as in the Markovian regime, for the hypothetical case of the Lorentzian zero-quantum lineshape, Eq. (88) gives the same expression for $s(t)$ as obtained in the semi-phenomenological R^2 treatment.[46] By making the same assumptions as were used to obtain Eq. (81) from Eq. (49), $k_D^{(0)}(\omega)$ is transformed to

$$k_D^{(0)}(\omega) = \left|\omega_D^{(n)}\right|^2 \frac{1}{\alpha + i\omega}, \tag{89}$$

where $\alpha^{-1} = T_2^{ZQ}$. The inverse Fourier transform of Eq. (88) using this expression for $k_D^{(0)}(\omega)$ yields

$$s(t) = e^{-\frac{1}{2}\alpha t}\left(\cos \Omega t + \frac{\alpha}{2\Omega} \sin \Omega t\right), \tag{90}$$

where

$$\Omega^2 = \frac{1}{6}\left|\omega_D^{(n)}\right|^2 - \frac{1}{4}\alpha^2. \tag{91}$$

Interestingly, the R^2 exchange in a system consisting of only two ^{13}C nuclei (in the absence of any protons) is described by the non-Markovian kinetic equation (34) exactly. This is a trivial consequence of the fact that the $R_I(t)$ term neglected in the derivation of this equation consists solely of zero-quantum coherences.

In order to test the validity of Eqs. (87) and (88) in the non-Markovian regime, we compared the results obtained through these equations with the results obtained by the direct simulations of the exchange, using CO–CO ^{13}C pair as the model system. Fig. 10 shows the signal $s(t)$ computed with both methods for the $n = 0$ rotational resonance condition (which is allowed by the presence of large ^{13}C CSAs). The direct simulation method is expected to produce physically accurate results only for a certain initial period of the exchange, the duration of which is limited by the number of protons included in the simulation. As one can see, the exchange curves computed with the two methods are identical until the point when the direct method curve starts to stray to its stationary value, suggesting that the curve computed through Eqs. (87) and (88) is physically accurate for a significant part of the exchange process, possibly even for the entire time of exchange. Simulations with the fewer protons in the system produce progressively smaller intervals over which the two methods give identical results.

Figure 11 compares $S(\omega)$ spectra computed for different values of the dipolar C–C coupling in the same system

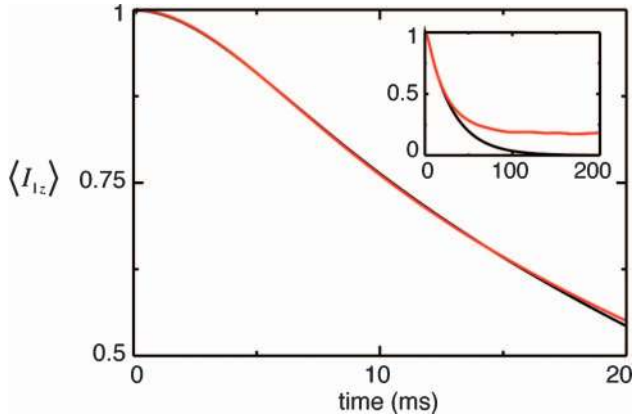

FIG. 10. Non-Markovian magnetization exchange during R^3-PDSD in a CO–CO pair at the exact $n = 0$ rotational resonance computed through Eq. (87) (black) and by the direct method (red) for a single crystallite. The long-term behavior is shown on the inset. The parameters of the Hamiltonian are as for the {Gly1–CO, Val3–CO} pair in GGV, except that the dipolar C–C coupling is scaled by a factor of 8 and the ^{13}C isotropic chemical shift difference is set to zero. Ten nearest protons are included in the system. Magnetizations are normalized to give a unit signal at $t = 0$. The angle between the C–C axis and the rotor axis is 45°. The spinning frequency is 10 kHz; the ^{1}H RF field is 60 kHz. Using Eq. (88) instead of the iteration through Eq. (87), gives essentially the same result.

at the $n = 1$ rotational resonance condition with the ^{13}C CSA effects neglected. The spectra obtained with the two methods are very similar, although not identical. Analogous simulations for other systems resulted in even larger differences between the two methods, possibly indicating an insufficient number of protons included in the simulations with the direct method, or even a limited validity of the basic equation (34).

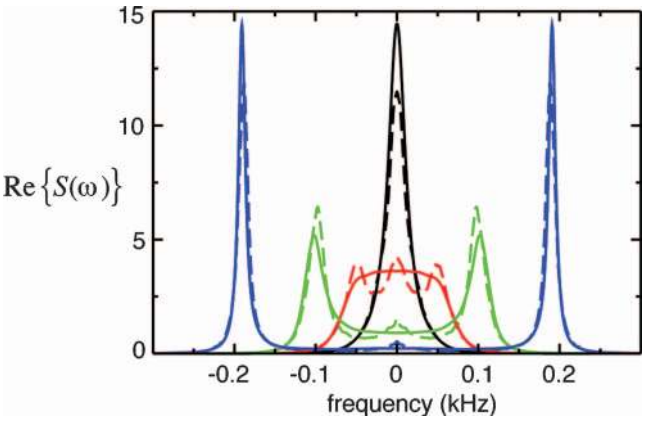

FIG. 11. Non-Markovian magnetization exchange during R^3-PDSD in a hypothetical ^{13}C pair at the exact $n = 1$ rotational resonance computed through Eq. (87) (solid lines) and by the direct method (dashed lines) for different scaling values applied to the dipolar C–C coupling. The spectra are shown instead of the time-domain signal. The proton environment for the pair is as for the {Gly1–CO, Val3–CO} pair in GGV; the ^{13}C CSA difference is set to zero; the ^{13}C isotropic chemical shift difference is set to 10 kHz. The dipolar C–C coupling is scaled (relative to the GGV pair) by the factors of 1 (black), 2 (red), 4 (green), and 8 (blue). Ten nearest protons are included in the system. Magnetizations are normalized to give a unit signal at $t = 0$. The spectra computed by the direct method are obtained after applying baseline correction to the time-domain signal (in order to remove the singular peaks at $\omega = 0$). The angle between the C–C axis and the rotor axis is 45°. The spinning frequency is 10 kHz; the ^{1}H RF field is 60 kHz. Using Eq. (88) instead of the iteration through Eq. (87), gives essentially the same result.

A more detailed study of these differences is required to determine their origin.

Importantly, the results obtained with both methods above, while in relative agreement with each other, are qualitatively different from the results predicted by the semi-phenomenological treatment of R^2. Indeed, for large dipolar coupling values, Eq. (90) can be approximated as

$$s(t) \simeq e^{-\frac{1}{2}\alpha t} \cos \Omega t, \tag{92}$$

which predicts that the two peaks in $S(\omega)$ will not change their width and amplitude as the dipolar coupling is scaled. This is in a stark contrast with the results displayed in Fig. 11, supporting our conjecture regarding the inadequacy of the semi-phenomenological treatment of relaxation in R^2 experiments. A conclusive statement on this issue can be made only after comparing the simulations with the experiment.

E. The DARR model

It was suggested by Takegoshi *et al.*[18,47] that R^3-PDSD can be understood through essentially the same approach as used to describe most other recoupling sequences in solid-state NMR, i.e., through computing the average Hamiltonian for one modulation period (rotor cycle in this case) of the pulse sequence. The authors postulated that the ^{1}H–^{1}H homonuclear interactions are not essential for understanding the R^3-PDSD mechanism and proposed a three-spin system consisting of two ^{13}C nuclei and one proton to model this experiment theoretically. In the interaction frame defined by the RF term, and assuming that the RF field amplitude matches the spinning frequency, the first-order average Hamiltonian of this three-spin system differs from the rotational resonance Hamiltonian only by an additional chemical-shift-like term resulting from the C–H interaction recoupled by the applied RF field. Hence, the name DARR (dipolar-assisted rotational resonance) has been proposed for this experiment and for the proposed magnetization transfer mechanism.

The theoretical and experimental results presented in this work make it clear that both this term, as well as the model itself are inadequate for the description of R^3-PDSD. To further illustrate this point, we show in Fig. 12, the magnetization exchange curves computed for the following Hamiltonians: the three-spin model Hamiltonian used by Takegoshi *et al.*[18,47] (blue line), the extended version of this Hamiltonian obtained by adding two more protons to the spin system but with all ^{1}H–^{1}H interactions omitted (red line), same but with the total of 10 protons in the system (green), and, finally, the 10-proton case but with the normal ^{1}H–^{1}H interactions (black). As one can see, the homonuclear interactions are absolutely essential for R^3-PDSD. Without them, the dissipation of coherences required for relaxation (Eq. (34)) does not occur, making the exponential decay of the difference magnetization impossible. The DARR oscillations become attenuated with the addition of protons into the system in Fig. 12 because the R^3-recoupled C–H dipolar line width in this system becomes much larger than the C–C coupling. As the line is inhomogeneous, only a small portion of it is capable of producing the DARR effect.

Furthermore, not only one cannot neglect the ^{1}H–^{1}H couplings in order to simplify the Hamiltonian but also any attempts at using the standard average Hamiltonian description for the PDSD phenomenon are unlikely to be very efficacious. Indeed, the interaction frame PDSD Hamiltonian (Eq. (21)) is not periodic, which implies that its average Hamiltonian is different for every rotor cycle. The rotating frame Hamiltonian is periodic, but the series for its average Hamiltonian – the Magnus expansion – is unlikely to even converge for moderate spinning frequencies due to its large (relative to ω_R) size.[87] When the expansion does converge (at high spinning frequencies) and can be approximated by the second-order term, it would still be unclear what kind of spin dynamics this average Hamiltonian would generate, unless one resorts to the numerical computation of its propagator.

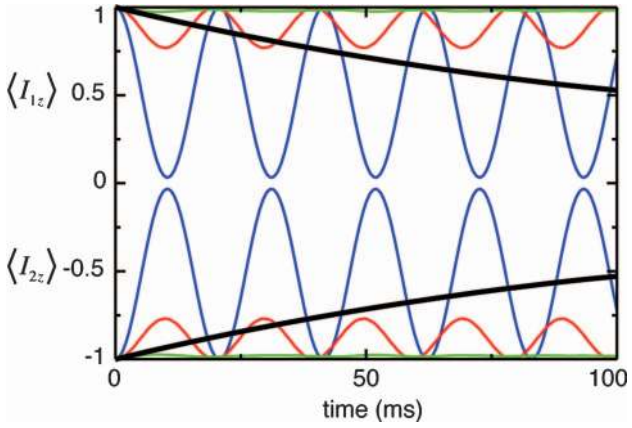

FIG. 12. DARR vs. R^3-PDSD. Magnetization exchange between the two ^{13}C nuclei simulated using different models (in a single crystallite). The blue, red, and green lines are for the DARR-type models (i.e., with the H–H dipolar couplings omitted from the Hamiltonians) containing 1, 3, and 10 protons, accordingly. For the blue line, the smaller of the two C–H couplings is also set to zero (as in the original DARR model[18,47]). The black line is for the full R^3-PDSD Hamiltonian in the system with 10 protons. The distance between the ^{13}C nuclei is 3.19 Å, with the internuclear axis tilted 18° from the rotor axis for the chosen crystallite orientation. The proton environment is that of a CO–CO pair in AGG. The spinning frequency and the ^{1}H-resonant RF field are 10 kHz. No CSAs are present. The ^{13}C chemical shifts difference (10.7 kHz for the blue and 10.8 kHz for all other lines) is optimized for the chosen crystallite orientation to give the maximum possible magnetization transfer in the vicinity of (but not on) the rotational resonance condition.

VII. SUMMARY AND CONCLUSIONS

Kinetic equations for the Markovian and non-Markovian regimes of proton-driven spin diffusion in rotating solids were derived using an original approach emphasizing dissipation of coherences as the source of the apparent irreversibility of the dynamics in the macroscopic systems. The non-Markovian equation has the form of a memory function equation, with the role of the memory function played by the correlation function. The theory describes MAS PDSD experiments with any form of periodic RF field applied at the ^{1}H frequency, including CW or no field (specific experiments are suggested to have compound names such as R^3-PDSD). Accurate expressions for the correlation functions and for the spin diffusion constants are given (Eqs. (47)–(49)). The effects of the CH and HH dipolar couplings enter these expressions through the Fourier components of the zero-quantum coherence lineshape. The theory predicts that the correlation functions and spin diffusion constants in multi-site PDSD can

be approximated by the corresponding quantities in the two-site PDSD, although the accuracy of this approximation may depend on the specific PDSD experiment.

Direct numerical simulations of the coherent PDSD dynamics (as described by the reversible Liouville-von Neumann equation) have been shown to fruitfully compliment the theory. On the grand scale, with the help of such simulations, PDSD in rotating solids emerges as an apparently irreversible macroscopic process that can be studied in full microscopic detail via reversible dynamics. A clean exponential decay can be observed in systems consisting of only 12 spins. As a consequence, PDSD suggests itself as a unique model for gaining insights into various issues of fundamental importance in the relaxation theory and other physical theories. On a smaller scale, such computations can be used to simulate important details of the spin diffusion dynamics in both Markovian and non-Markovian regime, corroborating and clarifying results obtained through the relaxation theory of spin diffusion. In particular, these simulations reveal the initial chaotic phase of the dynamics, which is traditionally considered inaccessible through the relaxation theory. The main limitation of this approach is that, due to the finite size of the system, the apparent macroscopic behavior stops after a certain degree of transfer is reached. As a result, the reversible model can be used to accurately simulate only a certain initial period of the magnetization exchange in any real physical system. Nevertheless, an accurate value for the spin diffusion constant can be usually obtained (from this initial period) through direct simulations of PDSD in systems of two ^{13}C nuclei and about ten ^{1}H nuclei from their nearest environment. The spin diffusion constant can be also obtained through equations given by the relaxation theory, using a correlation function computed through the simulations of the full quantum dynamics of the zero quantum coherence decay in the same systems. The constants resulting from these two approaches ("direct" and "spectral densities") are shown to be in excellent agreement with each other. The 2D R^3-PDSD experiments performed on the model compounds showed that these computations are also in excellent agreement with the experiment, with the model error of only about 0.5% for all thee compounds.

The samples used in the PDSD experiments (serine, AGG, and GGV, each containing three ^{13}C nuclei) were prepared by diluting the labeled compounds with the natural abundance compounds in ratios of 1:9 or higher. Even at these dilutions, intermolecular magnetization exchange was very significant. In order to account for it, we had to simulate spin diffusion in systems containing 230–450 ^{13}C nuclei that were set up to model the random distribution of the labeled molecules on the crystal lattice. Had the measurements been performed in pure labebled compounds, the data would have been much easier to interpret quantitatively, and would have probably produced smaller model error. The following factors have also been found important for the accuracy of the model: corrections for vibrational averaging in directly bonded C–C and C–H pairs, ^{13}C isotropic chemical shifts and CSA tensors, dynamics of the -CH3, -NH3 groups, and the spin-lattice relaxation (for long mixing times).

Distances between directly bonded ^{13}C nuclei could be extracted from the data with the 95% confidence intervals of about $\pm 0.25\%$ (or ± 0.004 Å). Longer distances were less accurate and had larger confidence intervals. The main source of the error was traced to the loss of information due to the relayed transfer of magnetization between distant nuclei. This issue is likely to be resolved when the measurements are done in molecules with multiple ^{13}C sites (partly, through the presence of multiple geometric constraints), and when several PDSD data sets (for different ^{1}H RF fields and spinning frequencies) providing complementary information are available for the same molecule.

The estimate we obtained for the effective CA–CB distance in serine (1.532 ± 0.0035 Å) is likely to be the most accurate estimate of a dipolar coupling in a directly bonded C–C pair available to date. When compared with the estimate of this distance given by the diffraction methods (1.514 ± 0.002 Å), it yields the room temperature vibrational averaging correction of $+0.018 \pm 0.004$ Å. The effective C–H distance in the CA group we used in the simulations (1.12 Å) was estimated to be accurate within ± 0.007 Å. PDSD experiments can be easily designed to measure this and other directly bonded CH distances to even higher precision. The accurate knowledge of these distances would improve the accuracy of the C–C distance measurements performed in future PDSD experiments.

Simple qualitative analysis of numerically simulated zero-quantum lineshapes can be used to understand or design PDSD experiments for various applications. As an example, the MIRROR recoupling condition can be trivially understood in this context. Another important observation that can be made about the zero-quantum lineshapes is that they are never Lorentzian.

The non-Markovian kinetic equation can be transformed to the frequency domain, where it can be solved to various degrees of approximation. This approach was applied to the dynamics of exchange in rotational resonance, which is a special case in the relaxation theory of PDSD. The conventional semi-phenomenological treatment of relxation in the R^2 exchange has been shown to be equivalent to the assumption of the Lorentzian lineshape for the zero-quantum coherence spectrum in our PDSD theory. Since these lineshapes are never Lorentzian in real physical systems, it is expected that the conventional treatment of rotational resonance is likely to carry a significant model error that has not been previously recognized. The theory presented in this work appears to be a more accurate alternative, as it provides a natural, parameter-free description of the R^2 exchange dynamics. Predictions of this theory agreed well with the full quantum mechanical simulations of the R^2 exchange in the few simple model systems we considered. However, due to the possible limitations on the validity of the basic non-Markovian equation, a conclusive statement on this issue can be made only after an extensive comparison with the experiment.

ACKNOWLEDGMENTS

We are grateful to Dr. Marvin Bayro who allowed us to borrow the samples used for collection of the experimental data. M.V. is also grateful to Professor John S. Waugh and Dr. Vikram Bajaj for stimulating discussions at the early

stages of this work, to Dr. David Ruben for providing expertise on the homebuilt spectrometer hardware and software, and to Dr. Phil Costa for sharing his original idea of applying ^{1}H RF field to enhance proton-driven spin diffusion. This research was supported by the NIBIB through Grant Nos. EB-003151 and EB-002026.

APPENDIX A: EXPRESSION FOR THE CORRELATION FUNCTION

Substitution of Eq. (41a) into Eq. (40) yields

$$\Phi(t+\tau;\tau) = \frac{1}{4\left\|I_z^{(23)}\right\|^2} D(t+\tau)D(t)e^{-i(\tau\omega_\Delta^{\rm iso}+\phi(t+\tau)-\phi(t))} \times Tr\left(I_-^{(23)}U_{\rm H}(t+\tau,t)I_+^{(23)}U_{\rm H}^\dagger(t+\tau,t)\right)+{\rm c.c.}, \tag{A1}$$

where we used the identity

$$e^{i\varphi I_z}I_-e^{-i\varphi I_z} = e^{-i\varphi}I_-. \tag{A2}$$

Substitution of the expressions for $D(t)$ (Eqs. (6) and (13)), $e^{i\phi(t)}$ (Eq. (43)), and $G(t;\tau)$ (Eqs. (44) and (45)) into Eq. (A1), followed by the use of the identity $\|I_+^{(23)}\|^2 = 2\|I_z^{(23)}\|^2$ transforms Eq. (A1) into

$$\begin{aligned}\Phi(t+\tau;\tau) &= \frac{1}{12}\sum_q\sum_{k,m=-2}^{2}\sum_{l,n} D_{2,0}^{(k)}e^{ik\omega_R(t+\tau)}D_{2,0}^{(m)}e^{im\omega_R t}e^{-i\omega_\Delta^{\rm iso}\tau} \times C^{(n)*}e^{-in\omega_R(t+\tau)}C^{(l)}e^{il\omega_R t}e^{iq\omega_R t}G_q(\tau)+{\rm c.c.}\\ &= \frac{1}{12}\sum_q\sum_{k,m=-2}^{2}\sum_{l,n} D_{2,0}^{(k)}D_{2,0}^{(m)}C^{(l)}C^{(n)*} \times e^{i(k+m-n+l+q)\omega_R t}e^{i(k\omega_R-n\omega_R-\omega_\Delta^{\rm iso})\tau}G_q(\tau)+{\rm c.c},\end{aligned} \tag{A3}$$

Substituting $t \to t-\tau$ on both sides of the equation results in

$$\Phi(t;\tau) = \frac{1}{12}\sum_q\sum_{k,m=-2}^{2}\sum_{l,n} D_{2,0}^{(k)}D_{2,0}^{(m)}C^{(l)}C^{(n)*}e^{i(k+m-n+l+q)\omega_R t} \times e^{i(-m\omega_R-l\omega_R-q\omega_R-\omega_\Delta^{\rm iso})\tau}G_q(\tau)+{\rm c.c.} \tag{A4}$$

Now, instead of n and l, we will use two new indices, p and r, defined by the relations

$$k-n=p, \tag{A5}$$

$$k+m-n+l+q=r. \tag{A6}$$

This results in

$$\Phi(t;\tau) = \frac{1}{12}\sum_{p,q,r}\sum_{k,m=-2}^{2} D_{2,0}^{(k)}D_{2,0}^{(m)}C^{(r-p-m-q)}C^{(k-p)*}e^{ir\omega_R t} \times e^{i(p\omega_R-r\omega_R-\omega_\Delta^{\rm iso})\tau}G_q(\tau)+{\rm c.c.} \tag{A7}$$

The double sum over k and m can now be rearranged as a product of two sums:

$$\Phi(t;\tau) = \frac{1}{12}\sum_{p,q,r} e^{ir\omega_R t}e^{i(p\omega_R-r\omega_R-\omega_\Delta^{\rm iso})\tau}G_q(\tau) \times \left\{\sum_{k=-2}^{2}D_{2,0}^{(k)}C^{(k-p)*}\right\}\left\{\sum_{m=-2}^{2}D_{2,0}^{(m)}C^{(r-p-m-q)}\right\}+{\rm c.c.} \tag{A8}$$

Substitution of the quantities $\omega_D^{(n)}$ (defined by Eq. (48)) for these sums gives our final expression for the correlation function:

$$\Phi(t;\tau) = \frac{1}{2}\sum_{p,q,r}\omega_D^{(p)}\omega_D^{(p+q-r)*}e^{ir\omega_R t}e^{i(p\omega_R-r\omega_R-\omega_\Delta^{\rm iso})\tau} \times G_q(\tau)+{\rm c.c.} \tag{A9}$$

APPENDIX B: CORRELATION FUNCTIONS IN MULTI-SPIN DIFFUSION

For any two observables F and Q, which are assumed to commute with $H_0(t)$, the correlation function expression (Eq. (35)) can be transformed as follows:

$$\begin{aligned}\Phi_{FQ}(t;\tau) &= \frac{1}{\|F\|\|Q\|}Tr\left(F[H_I(t),\ [H_I(t-\tau),\ Q]]\right)\\ &= -\frac{1}{\|F\|\|Q\|}Tr\left([H_I(t),\ F][H_I(t-\tau),\ Q]\right)\\ &= -\frac{1}{\|F\|\|Q\|}Tr\left(U_0^\dagger(t)[H_1(t),\ F]U_0(t)U_0^\dagger(t-\tau) \times [H_1(t-\tau),\ Q]U_0(t-\tau)\right)\\ &= -\frac{1}{\|F\|\|Q\|}Tr\left([H_1(t),\ F]U_0(t,t-\tau) \times [H_1(t-\tau),\ Q]U_0^\dagger(t,t-\tau)\right).\end{aligned} \tag{B1}$$

With the Hamiltonian given by Eq. (20) and Q_z (Eq. (17)) as both F and Q, this leads to Eq. (38).

With $F=I_{kz}$, $Q=I_{lz}$, and the Hamiltonian given by Eq. (58), Eq. (B1) can be evaluated as follows:

$$\begin{aligned}\Phi_{kl}(t;\tau) &= -\frac{1}{\|I_{kz}\|^2}Tr\left([H_1(t),\ I_{kz}]U_0(t,t-\tau)[H_1(t-\tau),\ I_{lz}] \times U_0^\dagger(t,t-\tau)\right) = -\sum_{\substack{j(\neq k)\\ i(\neq l)}} D_{kj}(t)D_{li}(t-\tau)\frac{1}{\|I_{kz}\|^2}\\ &\times Tr\left(\left[I_x^{kj(23)},I_{kz}\right]U_0(t,t-\tau)\left[I_x^{li(23)},I_{lz}\right]U_0^\dagger(t,t-\tau)\right)\\ &= -\sum_{\substack{j(\neq k)\\ i(\neq l)}} D_{kj}(t)D_{li}(t-\tau)\frac{1}{\|I_{kz}\|^2}Tr\left(\left[I_x^{kj(23)},\ I_z^{kj(23)}\right]\right.\\ &\left.\times U_0(t,t-\tau)\left[I_x^{li(23)},\ I_z^{li(23)}\right]U_0^\dagger(t,t-\tau)\right)\\ &= \sum_{\substack{j(\neq k)\\ i(\neq l)}} D_{kj}(t)D_{li}(t-\tau)\frac{1}{\|I_{kz}\|^2} \times Tr\left(I_y^{kj(23)}U_0(t,t-\tau)I_y^{li(23)}U_0^\dagger(t,t-\tau)\right).\end{aligned} \tag{B2}$$

In the first step, we used the fact that $[I_x^{ij(23)}, I_{kz}]$ vanishes unless $i = k$ or $j = k$. In the second, we used

$$I_{kz} = \frac{1}{2}(I_{kz} - I_{jz}) + \frac{1}{2}(I_{kz} + I_{jz}) = I_z^{kj(23)} + I_z^{kj(14)}. \quad \text{(B3)}$$

Now, we will show that for the trace $Tr(I_y^{kj(23)} U_0(t, t-\tau) I_y^{li(23)} U_0^\dagger(t, t-\tau))$ to be distinct from zero, indices kj must be the same as li or il. We will first focus on the $I_+^{li(23)}$ component of $I_y^{li(23)}$

$$I_y^{li(23)} = \frac{1}{2}\left(-i I_+^{li(23)} + i I_-^{li(23)}\right) = \frac{1}{2}(-i I_{l+} I_{i-} + i I_{l-} I_{i+}), \quad \text{(B4)}$$

writing it out explicitly as a product of the constituent single-particle operators:

$$I_{l+} I_{i-} = \mathbf{1}^{(\mathrm{H})} I_{l+} I_{i-} \prod_{\substack{j \\ (\neq l, \neq i)}} \mathbf{1}^{(j)}, \quad \text{(B5)}$$

where $\mathbf{1}^{(\mathrm{H})}$ is the unit operator in the spin space of the protons, and

$$\mathbf{1}^{(j)} = I_{j\alpha} + I_{j\beta}, \quad \text{(B6)}$$

are the unit operators of the ^{13}C or other low-gamma nuclei. If the product in Eq. (B5) is expanded using Eq. (B6), we obtain

$$I_{l+} I_{i-} = \sum_\nu \mathbf{1}^{(\mathrm{H})} I_{l+} I_{i-} \prod_{\substack{j \\ (\neq l, \neq i)}} I_{j\sigma(\nu, j)}, \quad \text{(B7)}$$

where the sum is over all possible "diagonal" states of the system of all ^{13}C nuclei, except l and i, and $\sigma(\nu, j)$ is the state (α or β) of spin j in the state ν. Since $H_0(t)$ is diagonal in these α/β states,

$$U_0 I_{l+} I_{i-} U_0^\dagger = \sum_\nu B_\nu^{(\mathrm{H})} I_{l+} I_{i-} \prod_{\substack{j \\ (\neq l, \neq i)}} I_{j\sigma(\nu, j)}, \quad \text{(B8)}$$

where $B_\nu^{(\mathrm{H})}$ are some operators in the spin space of the protons. The matrix structure of the operators in Eq. (B8) can be easily visualized in a representation, where the states are ordered to make $H_0(t)$ block-diagonal (i.e., where the ^{1}H states are "faster" than the ^{13}C states).

Combining Eq. (B8) with the property of the trace of a direct matrix product,

$$Tr(A \otimes B) = Tr(A) Tr(B), \quad \text{(B9)}$$

we can evaluate the trace:

$$Tr(I_{k+} I_{j-} U_0 I_{l+} I_{i-} U_0^\dagger) = \sum_\nu Tr\left(B_\nu^{(\mathrm{H})}\right) \times Tr\left(I_{k+} I_{j-} I_{l+} I_{i-} \prod_{\substack{j \\ (\neq l, \neq i)}} I_{j\sigma(\nu, j)}\right). \quad \text{(B10)}$$

As one can see, this trace is distinct from zero only if $k = i$ and $j = l$. Analogously, $Tr(I_{k-} I_{j+} U_0 I_{l+} I_{i-} U_0^\dagger)$ is distinct from zero only if $k = l$ and $j = i$. The $I_-^{li(23)}$ component of $I_y^{li(23)}$ will obviously give the same selection rules (but in reverse order). Finally, returning to Eq. (B2), for the case when $k \neq l$, we obtain Eq. (60) using

$$I_y^{kl(23)} = -I_y^{lk(23)}. \quad \text{(B11)}$$

For the case when $k = l$, we obtain Eq. (61).

[1] N. Bloembergen, Physica **15**(3–4), 386 (1949).
[2] F. Castellani, B. van Rossum, A. Diehl, M. Schubert, K. Rehbein, and H. Oschkinat, Nature (London) **420**(6911), 98 (2002).
[3] F. Castellani, B. J. van Rossum, A. Diehl, K. Rehbein, and H. Oschkinat, Biochemistry **42**(39), 11476 (2003).
[4] S. G. Zech, A. J. Wand, and A. E. McDermott, J. Am. Chem. Soc. **127**(24), 8618 (2005).
[5] W. T. Franks, B. J. Wylie, H. L. F. Schmidt, A. J. Nieuwkoop, R. M. Mayrhofer, G. J. Shah, D. T. Graesser, and C. M. Rienstra, Proc. Natl. Acad. Sci. U.S.A. **105**(12), 4621 (2008).
[6] T. Manolikas, T. Herrmann, and B. H. Meier, J. Am. Chem. Soc. **130**(12), 3959 (2008).
[7] A. Loquet, B. Bardiaux, C. Gardiennet, C. Blanchet, M. Baldus, M. Nilges, T. Malliavin, and A. Boeckmann, J. Am. Chem. Soc. **130**(11), 3579 (2008).
[8] C. Wasmer, A. Lange, H. Van Melckebeke, A. B. Siemer, R. Riek, and B. H. Meier, Science **319**(5869), 1523 (2008).
[9] A. Lange, S. Luca, and M. Baldus, J. Am. Chem. Soc. **124**(33), 9704 (2002).
[10] A. Lange, K. Seidel, L. Verdier, S. Luca, and M. Baldus, J. Am. Chem. Soc. **125**(41), 12640 (2003).
[11] M. Aluas, C. Tripon, J. M. Griffin, X. Filip, V. Ladizhansky, R. G. Griffin, S. P. Brown, and C. Filip, J. Magn. Reson. **199**, 173 (2009).
[12] N. M. Szeverenyi, M. J. Sullivan, and G. E. Maciel, J. Magn. Reson. **47**(3), 462 (1982).
[13] D. Suter and R. R. Ernst, Phys. Rev. B **25**(9), 6038 (1982).
[14] B. H. Meier, "Polarization transfer and spin diffusion in solid-state NMR," in *Advances in Magnetic and Optical Resonance*, Vol. 18, edited by W. S. Warren (Academic Press, New York, 1994), pp. 1–116.
[15] J. Jeener, B. H. Meier, P. Bachmann, and R. R. Ernst, J. Chem. Phys. **71**(11), 4546 (1979).
[16] K. Wüthrich, *NMR of Proteins and Nucleic Acids* (John Wiley and Sons, New York, 1986).
[17] P. Costa, M. Veshtort, and R. G. Griffin, in *39th Experimental NMR Conference*, Asilomar, Pacific Grove, CA, March 22–27, 1998.
[18] K. Takegoshi, S. Nakamura, and T. Terao, Chem. Phys. Lett. **344**, 631 (2001).
[19] C. R. Morcombe, V. Gaponenko, R. A. Byrd, and K. W. Zilm, J. Am. Chem. Soc. **126**(23), 7196 (2004).
[20] T. G. Oas, R. G. Griffin, and M. H. Levitt, J. Chem. Phys. **89**, 692 (1988).
[21] A. Bennett, R. G. Griffin, and S. Vega, in *NMR Basic Principles and Progress* (Springer-Verlag, Berlin, 1994), Vol. 33, pp. 1–77.
[22] A. E. Bennett, L. Becerra, and R. G. Griffin, J. Chem. Phys. **100**, 812 (1994).
[23] A. E. Bennett, J. Ok, R. G. Griffin, and S. Vega, J. Chem. Phys. **96**, 8624 (1992).
[24] M. Hohwy, C. M. Rienstra, C. P. Jaroniec, and R. G. Griffin, J. Chem. Phys. **110**(16), 7983 (1999).
[25] Y. K. Lee, N. D. Kurur, M. Helmle, O. G. Johannessen, N. C. Nielsen, and M. H. Levitt, Chem. Phys. Lett. **242**, 304 (1995).
[26] G. De Paëpe, M. J. Bayro, J. Lewandowski, and R. G. Griffin, J. Am. Chem. Soc. **128**, 1776 (2006).
[27] G. De Paëpe, J. R. Lewandowski, and R. G. Griffin, J. Chem. Phys. **128**, 124503 (2008).
[28] G. De Paëpe, J. R. Lewandowski, A. Loquet, A. Böckmann, and R. G. Griffin, J. Chem. Phys. **129**, 245101 (2008).
[29] I. Scholz, M. Huber, T. Manolikas, B. H. Meier, and M. Ernst, Chem. Phys. Lett. **460** (1–3), 278 (2008).
[30] P. R. Costa, Ph.D. thesis, Massachusetts Institute of Technology, 1996.
[31] M. J. Bayro, M. Huber, R. Ramachandran, T. C. Davenport, B. H. Meier, M. Ernst, and R. G. Griffin, J. Chem. Phys. **130**(11), 114506 (2009).
[32] R. Kubo, M. Toda, and N. Hashitsume, *Statistical Physics II: Nonequilibrium Statistical Mechanics*, 2nd ed. (Springer, New York, 1991).
[33] R. Zwanzig, J. Chem. Phys. **33**(5), 1338 (1960).
[34] D. Suter and R. R. Ernst, Phys. Rev. B **32**(9), 5608 (1985).
[35] P. M. Henrichs, M. Linder, and J. M. Hewitt, J. Chem. Phys. **85**(12), 7077 (1986).

[36]A. Kubo and C. A. McDowell, J. Chem. Soc., Faraday Trans. 1 **84**(11), 3713 (1988).
[37]M. Veshtort and R. G. Griffin, J. Magn. Reson. **178**, 248 (2006).
[38]J. N. Dumez and L. Emsley, Phys. Chem. Chem. Phys. **13**(16), 7363 (2011).
[39]I. Kuprov, J. Magn. Reson. **195**(1), 45 (2008).
[40]I. Kuprov, N. Wagner-Rundell, and P. J. Hore, J. Magn. Reson. **189**(2), 241 (2007).
[41]J. N. Dumez, M. C. Butler, and L. Emsley, J. Chem. Phys. **133**(22), 224501 (2010).
[42]M. C. Butler, J. N. Dumez, and L. Emsley, Chem. Phys. Lett. **477**(4–6), 377 (2009).
[43]J. L. Lebowitz, Phys. Today **46**(9), 32 (1993).
[44]F. Haake, *Quantum Signatures of Chaos*, 2nd ed. (Springer, New York, 2000).
[45]W. H. Zurek, Rev. Mod. Phys. **75**(3), 715 (2003).
[46]M. H. Levitt, D. P. Raleigh, F. Creuzet, and R. G. Griffin, J. Chem. Phys. **92**, 6347 (1990).
[47]K. Takegoshi, S. Nakamura, and T. Terao, J. Chem. Phys. **118**(5), 2325 (2003).
[48]A. Abragam, *Principles of Nuclear Magnetism* (Oxford University Press, New York, 1961).
[49]M. Goldman, J. Magn. Reson. **149**(2), 160 (2001).
[50]M. M. Maricq and J. S. Waugh, J. Chem. Phys. **70**(7), 3300 (1979).
[51]J. Herzfeld and A. Berger, J. Chem. Phys. **73**, 6021 (1980).
[52]D. P. Raleigh, M. H. Levitt, and R. G. Griffin, Chem. Phys. Lett. **147**, 71 (1988).
[53]M. G. Colombo, B. H. Meier, and R. R. Ernst, Chem. Phys. Lett. **146**, 189 (1988).
[54]E. Y. Chekmenev, R. Z. Xu, M. S. Mashuta, and R. J. Wittebort, J. Am. Chem. Soc. **124**(40), 11894 (2002).
[55]D. J. States, R. A. Haberkorn, and D. J. Ruben, J. Magn. Reson. **48**(2), 286 (1982).
[56]G. M. Sheldrick, Acta Crystallogr. A **46**, 467 (1990).
[57]M. Bak and N. C. Nielsen, J. Magn. Reson. **125**, 132 (1997).
[58]M. Veshtort, Ph.D. dissertation, Massachusetts Institute of Technology, 2003.
[59]T. J. Kistenmacher, G. A. Rand, and R. E. Marsh, Acta Crystallogr. B: Struct. Crystallogr. Cryst. Chem. **30**, 2573 (1974).
[60]E. R. Henry and A. Szabo, J. Chem. Phys. **82**(11), 4753 (1985).
[61]F. H. Allen, Acta Crystallogr. B: Struct. Sci. **42**, 515 (1986).
[62]M. Ottiger and A. Bax, J. Am. Chem. Soc. **120**(47), 12334 (1998).
[63]D. A. Case, J. Biomol. NMR **15**(2), 95 (1999).
[64]J. Lorieau and A. E. McDermott, Magn. Reson. Chem. **44**(3), 334 (2006).
[65]B. J. Gross and A. E. McDermott, J. Magn. Reson. **185**(1), 12 (2007).
[66]J. S. Lee and A. K. Khitrin, Concepts Magn. Reson. Part A **32A**(1), 56 (2008).
[67]J. J. Chang, R. G. Griffin, and A. Pines, J. Chem. Phys. **60**(6), 2561 (1974).
[68]R. A. Haberkorn, R. E. Stark, H. Vanwilligen, and R. G. Griffin, J. Am. Chem. Soc. **103**(10), 2534 (1981).
[69]A. Naito, S. Ganapathy, P. Raghunathan, and C. A. Mcdowell, J. Chem. Phys. **79** (9), 4173 (1983).
[70]T. G. Oas, C. J. Hartzell, T. J. Mcmahon, G. P. Drobny, and F. W. Dahlquist, J. Am. Chem. Soc. **109**(20), 5956 (1987).
[71]N. Asakawa, S. Kuroki, H. Kurosu, I. Ando, A. Shoji, and T. Ozaki, J. Am. Chem. Soc. **114**(9), 3261 (1992).
[72]C. H. Ye, R. Q. Fu, J. Z. Hu, L. Hou, and S. W. Ding, Magn. Reson. Chem. **31**(8), 699 (1993).
[73]T. Kameda, N. Takeda, S. Kuroki, H. Kurosu, S. Ando, I. Ando, A. Shoji, and T. Ozaki, J. Mol. Struct. **384**(1), 17 (1996).
[74]Y. F. Wei, D. K. Lee, and A. Ramamoorthy, J. Am. Chem. Soc. **123**(25), 6118 (2001).
[75]T. M. Duncan, *Compilation of Chemical Shift Anisotropies* (Farragut, Chicago, 1990).
[76]K. Beshah and R. G. Griffin, J. Magn. Reson. **84**(2), 268 (1989).
[77]K. Beshah, E. T. Olejniczak, and R. G. Griffin, J. Chem. Phys. **86**(9), 4730 (1987).
[78]J. R. Long, B. Q. Sun, A. Bowen, and R. G. Griffin, J. Am. Chem. Soc. **116**, 11950 (1994).
[79]J. R. Long, R. Ebelhauser, and R. G. Griffin, J. Phys. Chem. A **101**(6), 988 (1997).
[80]Y. Ishii, T. Terao, and S. Hayashi, J. Chem. Phys. **107**(8), 2760 (1997).
[81]E. V. Boldyreva, E. N. Kolesnik, T. N. Drebushchak, H. Ahsbahs, J. A. Beukes, and H. P. Weber, Z. Kristallogr. **220**(1), 58 (2005).
[82]H. H. Sun, L. K. Sanders, and E. Oldfield, J. Am. Chem. Soc. **124**(19), 5486 (2002).
[83]B. J. Wylie, L. J. Sperling, H. L. Frericks, G. J. Shah, W. T. Franks, and C. M. Rienstra, J. Am. Chem. Soc. **129**(17), 5318 (2007).
[84]D. P. Raleigh, G. S. Harbison, T. G. Neiss, J. E. Roberts, and R. G. Griffin, Chem. Phys. Lett. **138**(4), 285 (1987).
[85]Z. H. Gan and D. M. Grant, Mol. Phys. **67**(6), 1419 (1989).
[86]D. P. Raleigh, F. Creuzet, S. K. Das Gupta, M. H. Levitt, and R. G. Griffin, J. Am. Chem. Soc. **111**, 4502 (1989).
[87]F. Casas, J Phys A: Math Theor **40**(50), 15001 (2007).